Journal of South American Earth Sciences 98 (2020) 102391

Contents lists available at ScienceDirect

Journal of South American Earth Sciences

journal homepage: www.elsevier.com/locate/jsames

The Neoproterozoic basement of the Sauce Chico Inlier (Ventania System): Geochemistry and U–Pb geochronology of igneous rocks with African lineage in central-eastern Argentina

Carlos A. Ballivián Justiniano[a], Miguel A.S. Basei[b], Ana M. Sato[c], Pablo D. González[d], Manuela E. Benítez[e], Mabel E. Lanfranchini[e,*]

[a] Consejo Nacional de Investigaciones Científicas y Técnicas (CONICET). Instituto de Recursos Minerales (INREMI), Universidad Nacional de La Plata–Comisión de Investigaciones Científicas de la Provincia de Buenos Aires, Calle 64 esquina 120, 1er piso, C.P. 1900, La Plata, Argentina
[b] Conselho Nacional de Desenvolvimento Científico e Tecnológico (CNPq). Centro de Pesquisas Geocronológicas (CPGeo), Instituto de Geociências, Universidade de São Paulo, Cidade Universitária, Rua do Lago 562, CEP 05508-080, São Paulo, Brazil
[c] Consejo Nacional de Investigaciones Científicas y Técnicas (CONICET). Centro de Investigaciones Geológicas (CIG), CONICET–Universidad Nacional de La Plata, Diagonal 113 N° 275, C.P. B1904DPK, La Plata, Argentina
[d] Consejo Nacional de Investigaciones Científicas y Técnicas (CONICET). Instituto de Investigación en Paleobiología y Geología (IIPG), Universidad Nacional de Río Negro–CONICET, Av. Roca N° 1242, C.P. R8332EXZ, General Roca, Argentina
[e] Comisión de Investigaciones Científicas de la Provincia de Buenos Aires (CIC). Instituto de Recursos Minerales (INREMI), Universidad Nacional de La Plata–CIC, Calle 64 esquina 120, 1er piso, C.P. 1900, La Plata, Argentina

ARTICLE INFO

Keywords:
LA-ICP-MS U–Pb zircon dating
Sm–Nd isotope data
Sierra de la Ventana Belt
Dom Feliciano Belt
Gariep Belt

ABSTRACT

This study describes the geology, geochemistry, and LA-ICP-MS U–Pb geochronology of igneous rocks that crop out in the Sauce Chico Inlier (SCI) and constitute the Neoproterozoic basement of the Ventania System, Argentina. Magmatism registered in the SCI has developed in two phases. The first phase, of Tonian age, is represented by rift-related calc-alkaline and alkaline granites with ages of 783.8 ± 3.7 Ma ($\varepsilon Nd_{(t)} = -7.20$) and 776.5 ± 4.7 Ma ($\varepsilon Nd_{(t)} = +1.65$), respectively. This phase would be related to the break-up of the Rodinia supercontinent and subsequent opening of the Adamastor Ocean. In the Dom Feliciano Belt of southern Brazil and eastern Uruguay, the Tonian magmatism is represented in the Cerro Olivo Complex of the Punta del Este Terrane and in basement inliers of the Pelotas Batholith. The second phase, of Ediacaran age, started with the intrusion of syn-orogenic calc-alkaline granites (620.8 ± 5.8 Ma and 620.3 ± 2.5 Ma; $\varepsilon Nd_{(t)} = -9.94/-9.18$) and continued with the extrusion of post-orogenic alkaline (577.3 ± 3.9 Ma; $\varepsilon Nd_{(t)} = -6.29$) and calc-alkaline (543.6 ± 4.0 Ma; $\varepsilon Nd_{(t)} = -3.38$) acid volcanic rocks. This phase would be related to the closure of the Adamastor Ocean, generation of a magmatic arc along the western margin of the Kalahari Craton, and collision between this and the Río de la Plata Craton. A post-collisional magmatism would have developed due to orogenic collapse (< 580 Ma). With the exception of the Tonian alkaline granite, in the remaining SCI igneous rocks, the juvenile component becomes more important as the crystallization age decreases. The available Nd model ages are between 1.80 and 1.14 Ga and suggest a mixing of older crust with juvenile material. The tectonic evolution of the Ventania System basement is consistent with that observed in the Dom Feliciano Belt and its African counterparts. We present here the first evidence of Tonian magmatism in the Ventania System basement. The results presented here also confirm those obtained previously by other authors. Zircon cores from the SCI igneous rocks have U–Pb inherited ages between *ca.* 1200 and 900 Ma that could be indicative of a lineage with the Gariep Belt and its Namaqua basement in southwestern Africa.

1. Introduction

The Gondwana supercontinent was formed from cratonic nuclei which were amalgamated by mobile belts during the Neoproterozoic–Early Palaeozoic (Fig. 1). In Southwest Gondwana, the most important orogenic activity was related to the closure of the

* Corresponding author. Instituto de Recursos Minerales (INREMI), Universidad Nacional de La Plata–Comisión de Investigaciones Científicas de la Provincia de Buenos Aires, Calle 64 esquina 120, 1er piso, C.P. 1900, La Plata, Argentina.
E-mail address: lanfranchini@yahoo.com (M.E. Lanfranchini).

https://doi.org/10.1016/j.jsames.2019.102391
Received 28 June 2019; Received in revised form 10 October 2019; Accepted 10 October 2019
Available online 16 October 2019

Adamastor Ocean and the collision between the Río de la Plata-Paranapanema and Congo-Kalahari cratons of South America and Africa, respectively. This orogeny corresponds to the Brasiliano/Pan-African Cycle (*ca.* 900–500 Ma), which formed the Araçuaí-Ribeira-Dom Feliciano belts in eastern South America and the West Congo-Kaoko-Damara-Gariep-Saldania belts in western Africa (Fig. 1) (*e.g.*, Basei et al., 2008; Heilbron et al., 2008; Pedrosa-Soares et al., 2008). Besides the main cratonic nuclei, there were numerous minor crustal fragments, such as the Luis Alves, Curitiba, Encantadas, and Nico Pérez blocks in South America (*e.g.*, Oyhantçabal et al., 2018a; Passarelli et al., 2018) and possibly the Angola Block in Africa (*e.g.*, Porada and Berhorst, 2000; Frimmel et al., 2011).

The tectonic model presented by Basei et al. (2000) and Frimmel et al. (2011), and summarized by Basei et al. (2018), states that the subduction of the Adamastor Ocean occurred towards the east (present coordinates), generating a large magmatic arc along the western margins of the Congo-Kalahari cratons (*ca.* 640–600 Ma). The collision of the cratonic nuclei located on both sides of the Adamastor Ocean would have juxtaposed the magmatic arc to the passive margin deposits developed along the eastern margins of the Río de la Plata-Paranapanema cratons (*ca.* 600 Ma). The suture zone would be represented by shear zones of kilometric thickness developed over hundreds of kilometres (*e.g.*, Major Gercino, Dorsal do Canguçu, and Sierra Ballena shear zones). The current South Atlantic Ocean would have developed along a back-arc basin located east of the magmatic arc. The Dom Feliciano Belt of southern Brazil and eastern Uruguay (also known as Cuchilla Dionisio Belt in Uruguay), and its African counterparts (Fig. 2), namely the Kaoko, Damara, Gariep, and Saldania belts, record this tectonic model.

The Ventania System, also known as Sierra de la Ventana Belt or Sierras Australes of Buenos Aires, is a mountain belt of steep relief and low altitude ($\leq$ 1239 m.a.s.l.) located near the Atlantic coast in the central-eastern sector of Argentina (Figs. 2 and 3). It is composed of abundant Palaeozoic sedimentary rocks and scarce basement rocks (Fig. 3). Field relationships between the different basement units of the Ventania System are difficult to specify, mainly due to metamorphic and deformational overprint of Late Palaeozoic age that obliterated the original crosscutting relationships. Additionally, the basement rocks are almost entirely covered by modern deposits that surround the Ventania System, therefore, they crop out discontinuously. It should be noted that the Ventania System has no clear relationships with the Brasiliano/Pan-African orogenic belts mentioned above as well as with the southern limit of the Río de la Plata Craton.

The Ventania System crystalline basement is mainly composed of S-, A-, and I-type granites and peralkaline rhyolites (Rapela et al., 2003) (Fig. 3). The first K–Ar and Rb–Sr isotopic datings of these rocks allowed assigning them to the Brasiliano Orogenic Cycle (Cingolani and Varela, 1973; Varela and Cingolani, 1976) (Fig. 4). Subsequent U–Pb zircon dating constrained its crystallization ages to the Ediacaran–Middle Cambrian (Rapela et al., 2003; Tohver et al., 2012).

Rapela et al. (2003) suggested that the Neoproterozoic S-type magmatism of the Ventania System (607.0 $\pm$ 5.2 Ma) could be related to the closure of the Adamastor Ocean and be the southernmost exposure of the magmatism associated with the Dom Feliciano Belt (Fig. 2). Based on Nd model ages, these same authors indicated that the source of the S-type magmatism would be the Palaeoproterozoic rocks of the Tandilia System. The Ventania System basement has also been considered as the South American counterpart of the Saldania Belt (Rapela et al., 2003; Gregori et al., 2005; Chemale et al., 2011). In contrast, Tohver et al. (2012) related the Neoproterozoic–Middle Cambrian magmatism of the Ventania System to igneous events in the

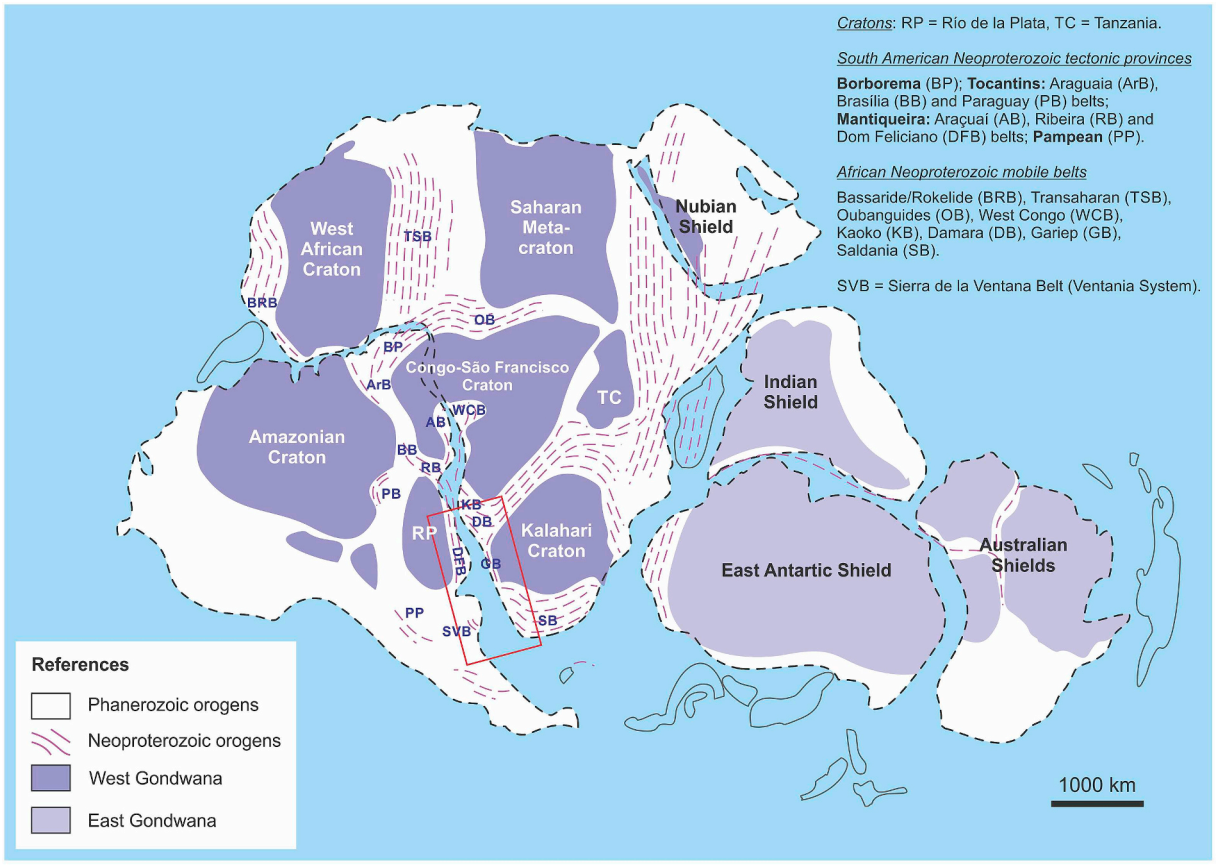

Fig. 1. Schematic geological map of the Gondwana supercontinent showing the main cratonic blocks and the Brasiliano/Pan-African orogenic belts of South America and Africa. The red rectangle shows the area represented in Fig. 2. Modified from Cordani et al. (2013). (For interpretation of the references to colour in this figure legend, the reader is referred to the Web version of this article.)

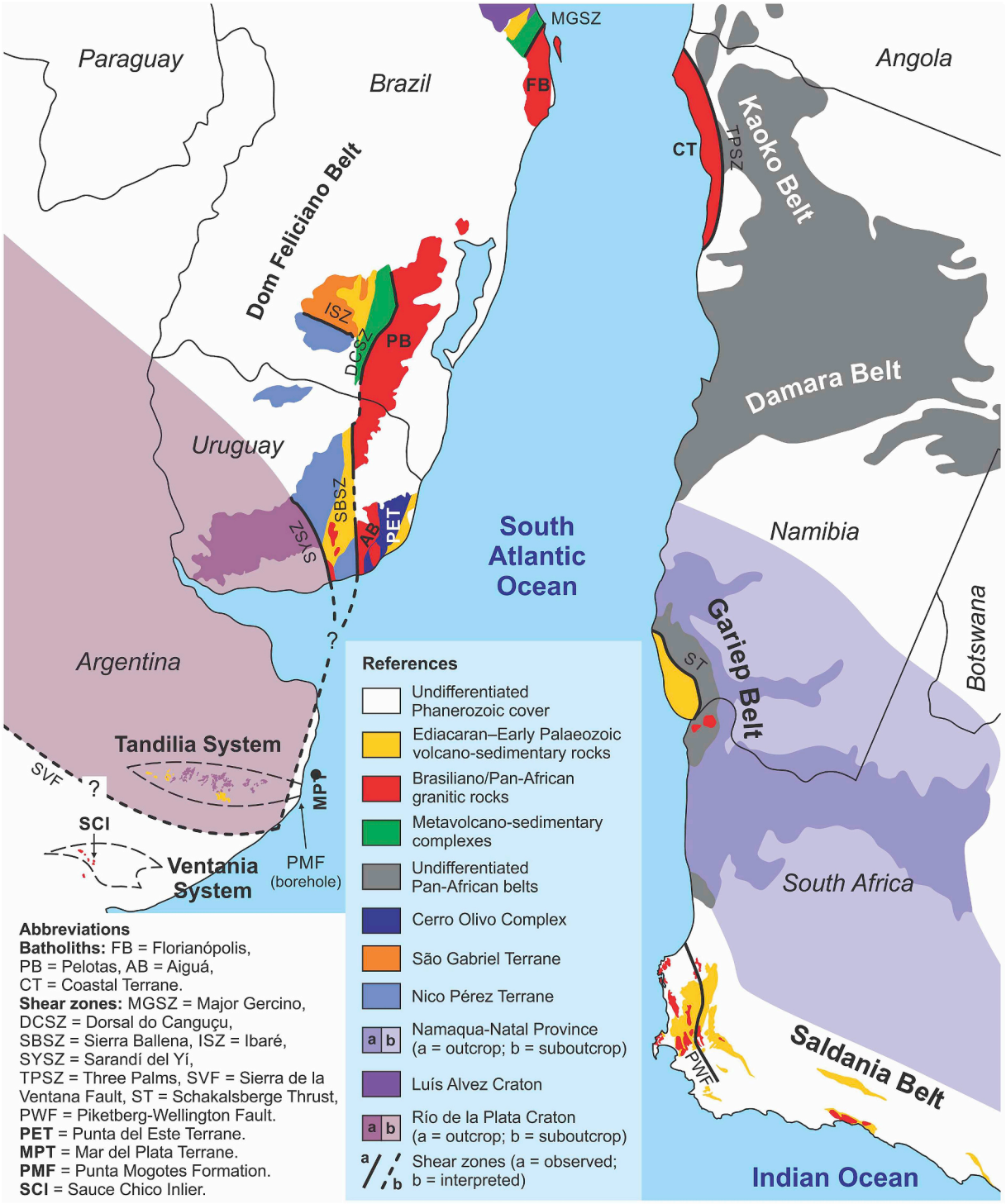

Fig. 2. Geological map of eastern South America and southwestern Africa in a Late Palaeozoic pre-drift reconstruction. The Palaeozoic to Cenozoic sedimentary covers on both sides of the South Atlantic Ocean were omitted. Modified from Basei et al. (2005), Cingolani (2011), Chemale et al. (2011), Frimmel et al. (2011), Rapela et al. (2011), Ramos et al. (2014), Philipp et al. (2016a), Thomas et al. (2016), and Oyhantçabal et al. (2018b).

Pampean Belt along the western margin of the Río de la Plata Craton.

Laser ablation inductively coupled plasma mass spectrometry (LA-ICP-MS) U–Pb zircon data, together with lithogeochemical and Sm–Nd whole rock analyses, were obtained for plutonic and volcanic rocks of the Neoproterozoic igneous-metamorphic basement of the Ventania System (Fig. 3). These rocks crop out at the Cerro Pan de Azúcar-Cerro del Corral area (37°56′18″ S, 62°10′18″ W), referred to as the Sauce Chico Inlier (SCI; Ballivián Justiniano et al., 2017). These results provide insights into the origin and evolution of the Neoproterozoic magmatism. For the first time, rocks of Tonian age are reported here for the Ventania System basement. We also attempt a comprehensive comparison and correlation between the Ventania System basement in Argentina and the Dom Feliciano Belt in southern Brazil and eastern Uruguay and their African counterparts, in order to discuss the Neoproterozoic palaeogeographic scenario prevailing along the southernmost Gondwana margin.

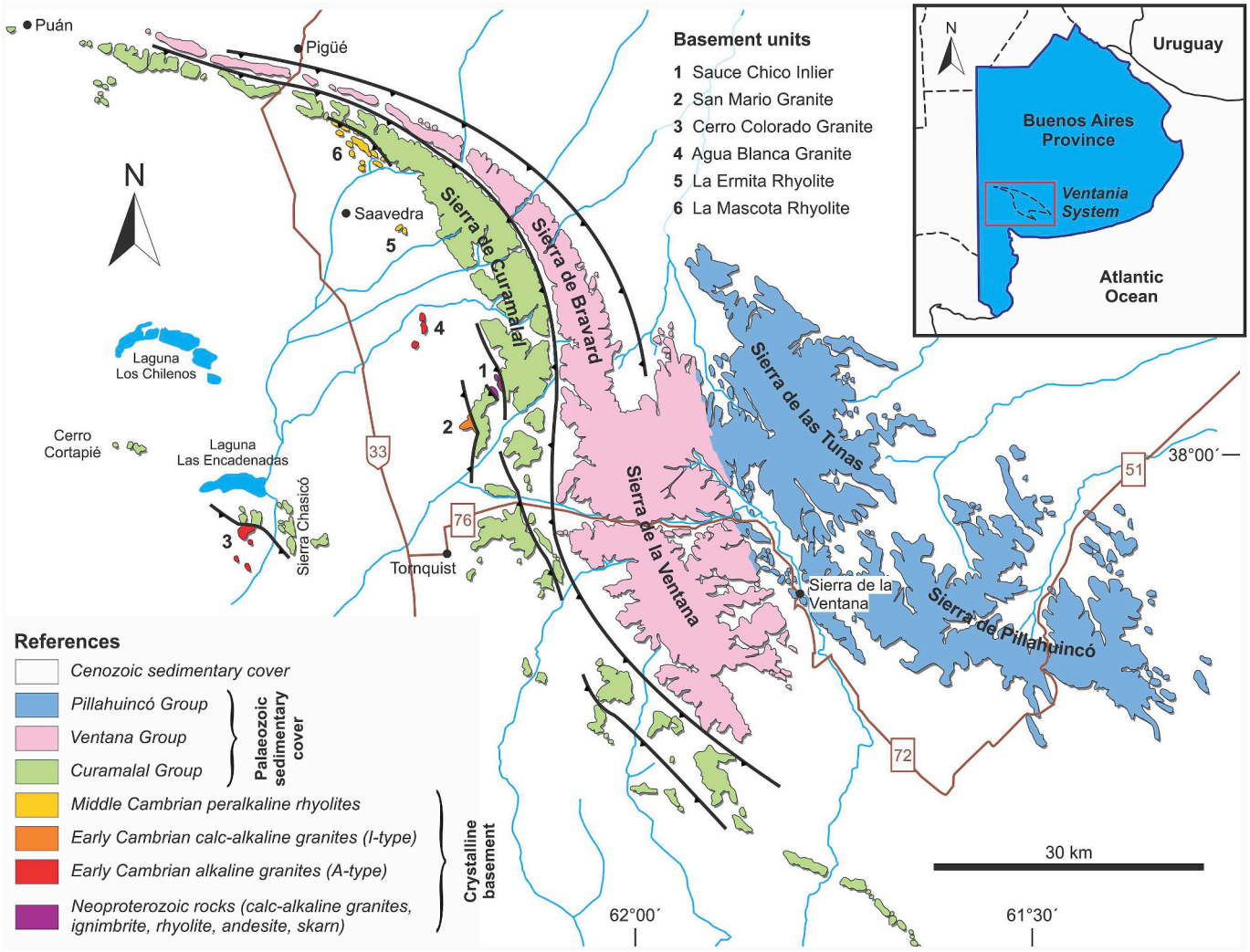

Fig. 3. Geological map of the Ventania System. Modified from Ramos et al. (2014).

2. Regional geological setting

The Ventania System is a Late Palaeozoic thick-skinned fold and thrust belt (von Gosen et al., 1990, 1991) located in the southwestern sector of the Buenos Aires Province, Argentina (Fig. 3). The belt is sigmoidal in shape and has an NW – SE orientation. It is surrounded by Mesozoic to Cenozoic deposits of the Chaco-Pampean Plain. The Ventania System is composed of scarce Neoproterozoic–Middle Cambrian basement rocks and abundant Palaeozoic sedimentary rocks. Geophysical and drilling data identified the offshore continuity of at least part of the Palaeozoic sedimentary sequence (Pángaro and Ramos, 2012; Pángaro et al., 2016; Prezzi et al., 2018).

The Ventania System basement crops out in the western sector of the system, along the western edge of Sierra de Curamalal and in the adjacent plain that extends to the west (Fig. 3). It is mainly composed of Neoproterozoic S-type granites, Early Cambrian alkaline (A_2-type) and calc-alkaline (I-type) granites, and Middle Cambrian peralkaline rhyolites (A_1-type) (Rapela et al., 2003). There are also outcrops of ignimbrites (González et al., 2004) and andesites (Kilmurray, 1968a) (Fig. 5). In the Neoproterozoic granites cropping out in the SCI, xenoliths of polymetamorphic sedimentary carbonate rocks (Loma Marcelo skarn; Ballivián Justiniano et al., 2017, 2019), metapelites, and orthogneisses were identified.

The Ventania System is essentially constituted by siliciclastic sedimentary rocks of Palaeozoic age included by Harrington (1947) in three groups: Curamalal (Late Cambrian–Ordovician), Ventana (Silurian–Devonian), and Pillahuincó (Late Carboniferous–Early Permian) (Fig. 3). The Curamalal and Ventana groups are similar due to their fining-upward sequence arrangement and depositional environment. Both of them are composed of basal conglomerates, abundant quartzites, and scarce cuspidal pelites deposited in a stable platform environment (Andreis et al., 1989). The Pillahuincó Group is composed of diamictites, conglomerates, arkoses, quartzites, pelites, and some tuff levels deposited in glacimarine and fluvio-deltaic environments (Andreis et al., 1989). Uriz et al. (2011) and Ramos et al. (2014) conducted provenance studies on detrital zircons of these three groups.

The crystalline basement and the Palaeozoic sedimentary cover of the Ventania System were deformed and metamorphosed together. The basement is mylonitized, whereas the Palaeozoic cover is folded and faulted.

The deformation age was determined by K–Ar dating of illite of the Mascota Formation (Curamalal Group) that gave ages between 282 ± 3 Ma and 257 ± 8 Ma (Varela et al., 1985; Buggisch, 1987). Subsequent palaeomagnetic studies carried out in the Tunas Formation (top unit of the Pillahuincó Group) revealed that the lower part of this unit was deposited, deformed, and remagnetized during the Early Permian (*e.g.*, Tomezzoli and Vilas, 1999; Tomezzoli, 2001). Deformation in the Ventania System could have even reached the Triassic (*e.g.*, Japas, 1987; Kollenz et al., 2017). Recent Rb–Sr dating of muscovite from ultramylonites suggests the existence of a deformation event of

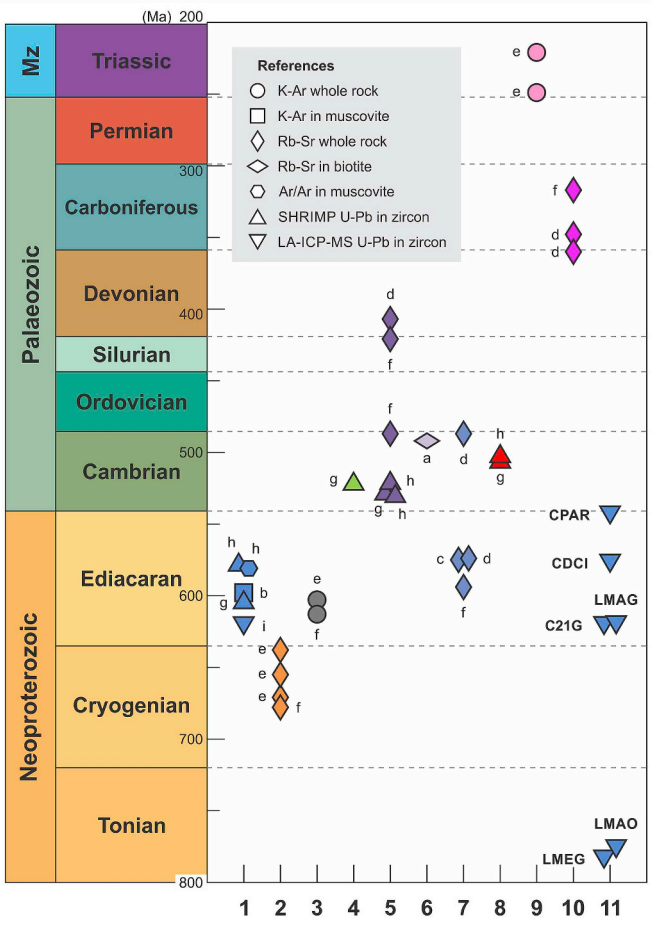

Fig. 4. Compilation of the published and newly obtained isotopic ages of the Ventania System basement rocks: **1** Sauce Chico Inlier (SCI) granites, **2** Cerro del Corral Ignimbrite (SCI), **3** Cerro Pan de Azúcar Andesite (SCI), **4** San Mario Granite, **5** Cerro Colorado Granite, **6** Agua Blanca Granite, **7** San Mario and Agua Blanca granites, **8** La Ermita Rhyolite, **9** La Mascota Rhyolite, **10** La Ermita and La Mascota rhyolites, **11** SCI plutonic and volcanic rocks (this work). 7 and 10 correspond, in each case, to Rb–Sr isochron ages determined from samples of two different units considered as one by the respective authors. In section 9, it is proposed to include all the Ventania System basement rocks in the Sauce Chico Complex, not only those that crop out in the homonymous inlier. **Abbreviations:** LMEG = Loma Meyer Granite, LMAO = Loma Marcelo Orthogneiss, C21G = Cerro 21 de Septiembre Granite, LMAG = Loma Marcelo Granite, CDCI = Cerro del Corral Ignimbrite, CPAR = Cerro Pan de Azúcar Rhyolite. **References: a** Borrello and Venier (1967), **b** Cazeneuve (1967), **c** Halpern et al. (1970), **d** Cingolani and Varela (1973), **e** Varela and Cingolani (1976), **f** Varela et al. (1990), **g** Rapela et al. (2003), **h** Tohver et al. (2012), **i** Ballivián Justiniano et al. (2019).

Late Devonian–Early Carboniferous age (Ballivián Justiniano et al., 2017).

Deformation and metamorphism are more intense in the western sector of the system, where conditions of temperature and pressure were those of the greenschist facies (von Gosen et al., 1990, 1991). Folds are tighter and overturned towards the NE (Schiller, 1930; Harrington, 1947; Suero, 1972). In the eastern sector of the system, the folding intensity is lower and the vergence of the geological structures is towards the W/SW. In the eastern tip of the system, conditions of metamorphism were those of the anchizone (von Gosen et al., 1990, 1991).

3. Geology of the Sauce Chico Inlier

In the Cerro Pan de Azúcar-Cerro del Corral area, the existence of Neoproterozoic rocks surrounded by younger ones of Early Palaeozoic age allowed Ballivián Justiniano et al. (2017) to name the area as Sauce Chico Inlier (Fig. 5). The name refers to the Sauce Chico Group, a lithostratigraphic unit defined by Cuerda et al. (1975) to gather the basement rocks of the area. The mylonitization of the crystalline basement occurred together with folding and faulting of the Palaeozoic sedimentary cover. The sedimentary rocks that overlie the SCI basement rocks form an anticline overturned towards the NE, which was affected by reverse faults of ductile nature. The Cerro Pan de Azúcar and Cerro del Corral constitute the SW and NE flanks, respectively, of the overturned anticline (Ballivián Justiniano et al., 2017). Along the fold axis, an erosive window, known as Abra Meyer Valley, allows observation of the basement rocks underlying the Early Palaeozoic sedimentary sequence. The NW–SE to N–S trending mylonitic foliation dips between 30 and 90° towards the SW/W and the associated stretching lineation dips between 42 and 52° towards the SSW (Fig. 5), whereas the kinematic indicators reveal reverse dextral shearing with a top-to-NNE hanging wall.

The SCI crystalline basement consists of mylonitic granites at Cerro del Corral, Cerro 21 de Septiembre, Loma Marcelo, and Loma Meyer; mylonitic rhyolites and/or dacites at Cerro Pan de Azúcar and Cerro del Corral; a meta-andesite body at Cerro Pan de Azúcar; and the Loma Marcelo skarn (Fig. 5). All of these rocks are deformed to a different extent and cut by quartz veins and veinlets.

U–Pb zircon datings revealed crystallization ages of 621.6 ± 2.2 Ma for the Loma Marcelo Granite (Ballivián Justiniano et al., 2019), 607.0 ± 5.2 Ma for the Cerro del Corral Granite (Rapela et al., 2003), and 580.8 ± 7.9 Ma for the Cerro Pan de Azúcar Granite (Tohver et al., 2012). Tohver et al. (2012) also reported a muscovite Ar/Ar age of 576 ± 5 Ma for the Cerro Pan de Azúcar Granite, which is call here as Loma Meyer Granite (Tohver, pers. com.). Previously, Varela et al. (1990) reported recalculated ages (from those determined by Varela and Cingolani (1976)) of 678 ± 30 Ma for the Cerro del Corral Ignimbrite (Rb–Sr, whole rock isochron) and 613 ± 30 Ma for the Cerro Pan de Azúcar Andesite (K–Ar, whole rock). Fig. 4 shows a compilation of the published isotopic ages of the Ventania System basement rocks.

The Early Palaeozoic sedimentary rocks that cover the Neoproterozoic basement of the SCI belongs to the La Lola and Mascota formations of the Curamalal Group (Harrington, 1947). These units crop out in Cerro Pan de Azúcar, Cerro del Corral, and Cerro del Hueco (Fig. 5). The La Lola Formation has a maximum thickness of 100 m and consists of reddish clast- and matrix-supported conglomerates with rounded to sub-rounded elongated pebbles of quartzites (with subordinate slates, quartz of veins, and rhyolites) up to 25 cm in diameter immersed in a well sorted coarse sand matrix (Harrington, 1947, 1972; Zavala et al., 2000). Pebbles of the La Lola Formation are much less deformed at Cerro Pan de Azúcar than at Cerro del Corral and Cerro del Hueco, having ellipsoidal shape and variable degree of flattening due to the ductile deformation occurred in the latter places (Schiller, 1930; Cucchi, 1966). The Mascota Formation, that overlies the La Lola Formation, has a maximum thickness of 200 m and consists of greyish, whitish, pinkish, and greenish quartzites of fine to very fine grain size, with cross-bedding and scarce massive pelites located towards the top of the unit (Harrington, 1947, 1972; Zavala et al., 2000). Quartz veins and veinlets cut the sedimentary rocks of the La Lola and Mascota formations. Modern deposits that fill the Abra Meyer Valley and dominate the adjacent plain are of aeolian and fluvial origin.

3.1. Cerro Pan de Azúcar and Loma Meyer

The mylonitic volcanic rocks of the northeastern slope of Cerro Pan de Azúcar underlie the Early Palaeozoic sedimentary cover and crop out scarcely due to the presence of hillside deposits (Fig. 6a). The Loma Meyer is a hill of 0.047 km^2 located at the foot of Cerro Pan de Azúcar and composed of mylonitic granites (Fig. 6a).

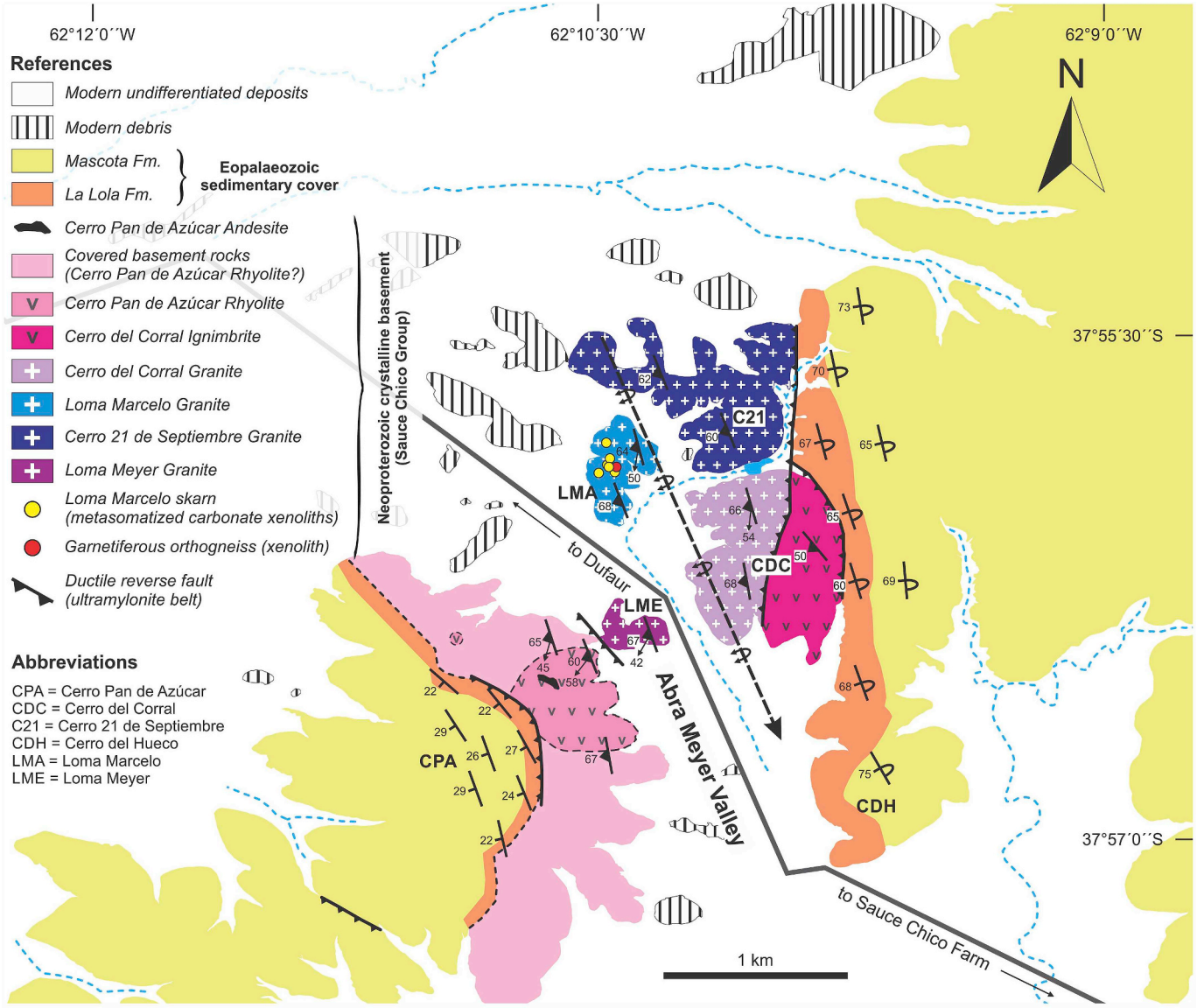

Fig. 5. Geological map of the Sauce Chico Inlier. Modified from Ballivián Justiniano et al. (2017).

The northeastern slope of Cerro Pan de Azúcar was considered as composed only by mylonitic granites by many authors. However, Kilmurray (1975) cited the presence of fine grain mylonites possibly derived from a porphyry, welded tuff, or rhyolite. Gregori et al. (2005) also recognized rocks of volcanic nature, which were classified as rhyolites according to their petrographic characteristics. We favour the idea that the volcanic rocks, possibly rhyolitic to dacitic ignimbrites, are the dominant basement rocks in Cerro Pan de Azúcar (Fig. 5).

Cobbold et al. (1986) and Gregori et al. (2005) interpreted the basement-Palaeozoic cover contact at Cerro Pan de Azúcar as a thrust fault with NE vergence. During fieldwork, the presence of greenish muscovite-bearing ultramylonites along the basement-Palaeozoic cover contact was observed. In our opinion, it would not be a thrust fault, but a reverse fault of a higher angle with N 20° W/60° SW orientation, developed under ductile conditions (Fig. 5). A fault with similar characteristics was identified between the mylonitic volcanic rocks of Cerro Pan de Azúcar and the mylonitic granites of Loma Meyer (N–S/57° W).

von Gosen et al. (1990) mentioned the presence of paragneisses at Cerro Pan de Azúcar and Ramos et al. (2014) quoted orthogneisses at Loma Meyer. In this last hill, we found small metapelitic xenoliths that look like a slate.

3.2. Cerro del Corral and Cerro 21 de Septiembre

At Cerro del Corral (Fig. 6b), mylonitic volcanic rocks are in tectonic contact with the La Lola Formation to the east and with mylonitic granites to the west, in both cases through N–S trending and west dipping ductile reverse faults (Figs. 5 and 6c). These ductile faults are marked by the presence of greenish muscovite-bearing ultramylonites. They converge towards the north, becoming a single fault with an N–S trend that tectonically juxtaposes the mylonitic granites of Cerro 21 de Septiembre next to the La Lola Formation (Fig. 5).

Rocks of the eastern part of Cerro del Corral were classified as rhyolites and rhyolitic porphyries by Kilmurray (1968a, 1968b, 1975) and later reinterpreted as rhyolitic to dacitic ignimbrites by González et al. (2004). At Cerro del Corral and Cerro del Hueco, the Early Palaeozoic sequence juxtaposed to the basement rocks is ductilely deformed. We found metapelitic xenoliths hosted in the granite of the western part of Cerro del Corral (similar to those found at Loma Meyer).

3.3. Loma Marcelo

The Loma Marcelo is a hill of 0.113 km^2 mainly composed of cataclastic and protomylonitic granites intercalated with highly foliated

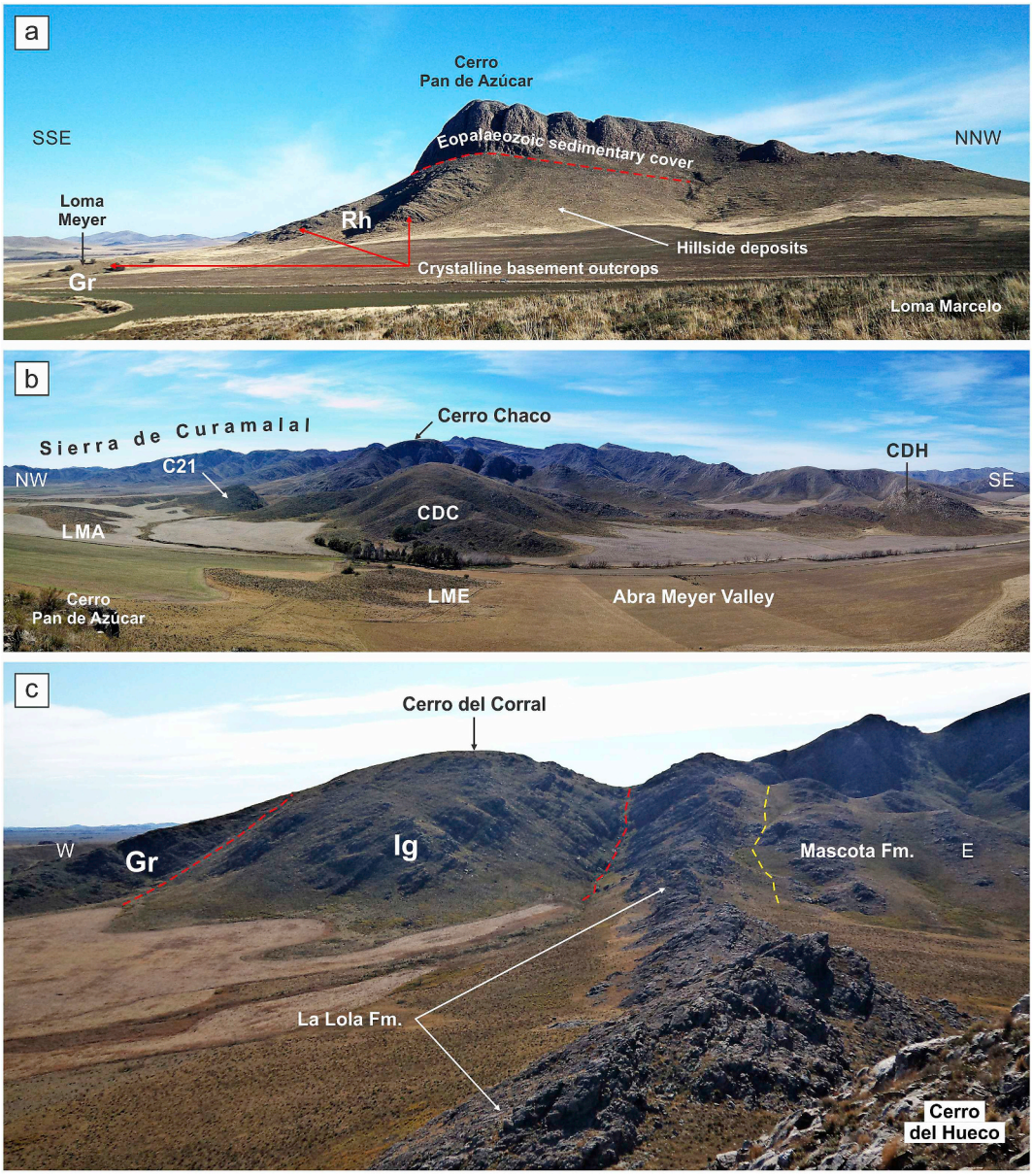

Fig. 6. a) View of Cerro Pan de Azúcar and Loma Meyer from the southern end of Loma Marcelo. The red dashed line marks the tectonic contact between the crystalline basement and the Early Palaeozoic sedimentary cover (Curamalal Group). **b)** Panoramic view of Loma Marcelo (LMA), Cerro 21 de Septiembre (C21), Cerro del Corral (CDC), Loma Meyer (LME), and Cerro del Hueco (CDH). The photograph was taken from Cerro Pan de Azúcar. **c)** View of Cerro del Corral and Cerro del Hueco. The red dashed line marks the tectonic contact between ignimbrite, granite, and the Early Palaeozoic sedimentary cover (Curamalal Group). The yellow dashed line marks the contact between the La Lola and Mascota formations. **Abbreviations:** Rh = rhyolite, Gr = granite, Ig = ignimbrite. (For interpretation of the references to colour in this figure legend, the reader is referred to the Web version of this article.)

belts of mylonitic granites (Fig. 5). Calc-silicate rocks crop out in the central-western sector of the hill (Ballivián Justiniano et al., 2017). They are aligned in an NNW–SSE trend along 175 m, parallel with the general trend of the mylonitic foliation. A metacarbonate rock crops out on the western side. The calc-silicate and metacarbonate rocks were characterized as calcic and magnesian skarns, respectively, and collectively referred to as Loma Marcelo skarn (Ballivián Justiniano et al., 2017). Granitic rocks surround the skarn outcrops (Fig. 5). An orthogneiss was identified next to the largest outcrop of the calcic skarn. Both the skarn and the orthogneiss are xenoliths incorporated during the intrusion of the granite.

4. Materials and methods

Twenty-six samples of the SCI basement rocks were analysed for petrography, lithogeochemistry (whole rock major and trace elements geochemistry), U–Pb geochronology, and/or Sm–Nd isotopic systematics.

During the petrographic study, in addition to a polarized light microscope, a FEI Quanta 200 scanning electron microscope, equipped with an EDAX SDD Apollo 40 X-ray dispersive energy probe, was used at the Laboratorio de Investigaciones de Metalurgia Física (LIMF), Universidad Nacional de La Plata, Argentina. Electron microprobe analyses were performed at the Laboratorio de Microscopía Electrónica y Análisis por Rayos X (LAMARX), Universidad Nacional de Córdoba, Argentina, with a JEOL Superprobe JXA-8230 microprobe. Crystals of garnet from the SCI mylonitic granites were analysed using a current acceleration of 15 kV, an electric current between 10 and 20 nA, and a beam diameter of 1–2 μm. Calibrations were performed using natural and synthetic standards.

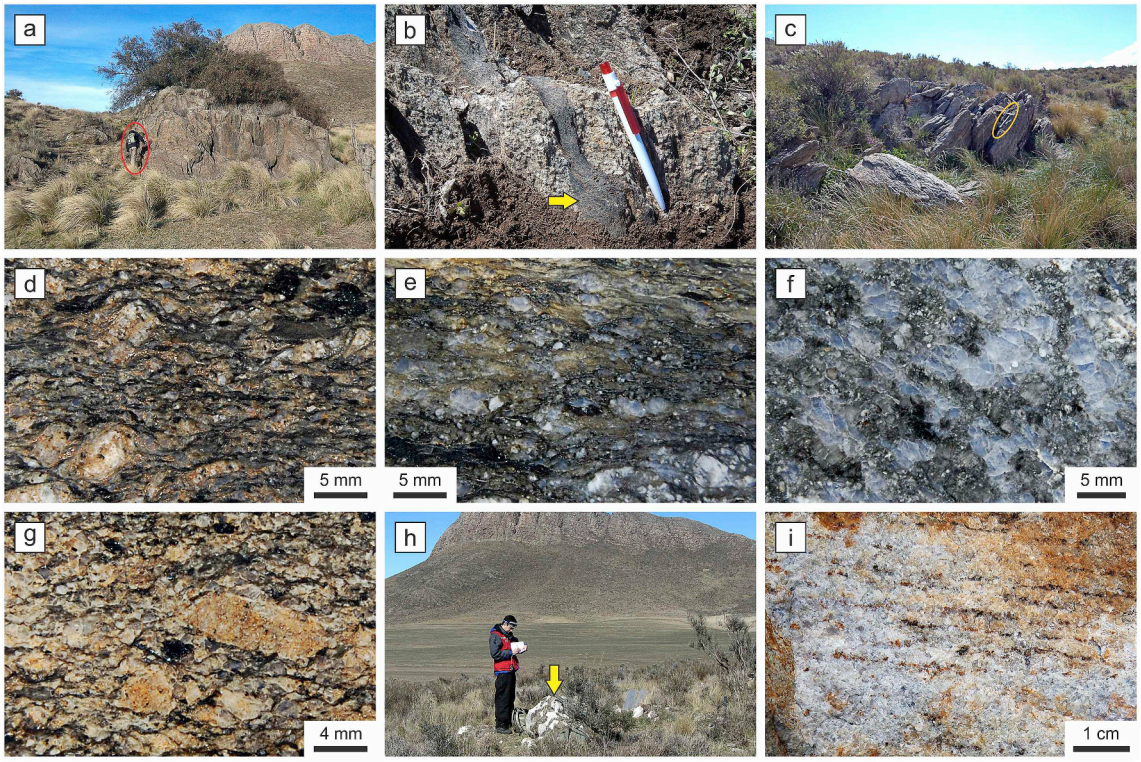

Fig. 7. a) Outcrop of the Loma Meyer Granite (the red oval indicates a person as a scale). **b)** Pelitic xenolith, indicated by the yellow arrow, foliated together with the Loma Meyer Granite (pen width = 1 cm). **c)** Outcrop of the Loma Marcelo Granite (the yellow oval indicates a hammer placed to show the scale). **d)** Loma Meyer Granite (polished hand sample, PHS). **e)** Cerro 21 de Septiembre Granite (PHS). **f)** Loma Marcelo Granite (PHS). **g)** Cerro del Corral Granite (PHS). **h)** Outcrop of the Loma Marcelo skarn indicated by the yellow arrow. **i)** Loma Marcelo Orthogneiss (PHS). (For interpretation of the references to colour in this figure legend, the reader is referred to the Web version of this article.)

Major and trace elements were analysed at Bureau Veritas Minerals Laboratories, ALS Global, and the geochemistry laboratory of the Centro de Investigaciones Geológicas (CIG, CONICET-UNLP). Major elements were determined by fused bead, acid digestion, and ICP-AES/MS. Trace elements were determined by lithium borate fusion prior to acid dissolution and ICP-MS. Carbon, sulphur, and fluorine were analysed at Bureau Veritas Minerals Laboratories. The C and S contents were determined by infrared detection following combustion in a LECO analyser, whereas the F content was determined by the potentiometric method with a LaF crystal membrane electrode.

Six samples were selected for LA-ICP-MS U–Pb zircon dating. Concentration and separation of zircon grains were done at the CIG and the Instituto de Recursos Minerales (INREMI, UNLP-CIC). Samples of 4–10 kg were crushed, washed, milled, and sieved. Heavy minerals were concentrated with a pan and then treated with common and neodymium magnets to concentrate the less magnetic fraction. Zircon grains were handpicked in alcohol under a binocular microscope. Selected zircon grains were mounted in epoxy resin and their internal structures were exposed by polishing for cathodoluminescence (CL) imagery and dating. The U–Pb ages were obtained at the Centro de Pesquisas Geocronológicas (CPGeo) of the Universidade de São Paulo, Brazil, with a Thermo Fisher Neptune LA multicollector ICP-MS equipped with a 193 Photon laser system, following the analytical method described by Souza et al. (2017). The operating conditions during the U–Pb analysis were the following: 6 Hz frequency, 9.98 J/cm^2 fluence, ablating for approximately 60 s, and 32 μm spot size. Each analysis consists of 60 sequential measurements performed in the ICP-MS: 15 with the laser off (measurement of instrumental blank) and 45 with the laser on (laser ablation on NIST-612 and GJ-1 standards or the analyte). Each measurement lasts approximately 1 s. Seven isotopes are measured simultaneously: ^{206}Pb, ^{208}Pb, ^{232}Th, and ^{238}U with Faraday cups and ^{202}Hg, ^{204}Pb, and ^{207}Pb with multiple ion counters. At the end of each sequence of measurements, the value of the instrumental blank is subtracted from each of the seven isotope signals. The isotope signal 235 is not measured but is mathematically obtained by dividing the isotope signal 238 by the relative abundance 238/235 (= 137.88). The participation of Hg from the transport gas in the isotope signal 204 is discounted from the latter by subtracting the following ratio: isotope signal 202/relative abundance 202/204 (= 4.355). The relative abundances 206/204, 207/204, and 208/204 are calculated using the partially corrected 207/206 ratio (age estimator) and the formulas of Stacey and Kramers (1975). The common Pb fraction (non-radiogenic) of the isotope signals 206, 207, and 208 is discounted by subtracting from each of them the isotope signal 204 multiplied by the relative abundances 206/204, 207/204, and 208/204, respectively. Before and after the analysis, blanks, NIST-612 synthetic standard, and GJ-1 zircon standard are measured. The analyses of the GJ-1 standard are repeated periodically every 10 min approximately in order to correct the errors and/or variations of the equipment in the following measurements. Jackson et al. (2004) reported a TIMS U–Pb age of 608.5 ± 0.4 Ma for the GJ-1 zircon standard. The LA-ICP-MS U–Pb age obtained for this standard at the CPGeo was 600.4 ± 0.8 Ma (Souza et al., 2017). The obtained data in the ICP-MS were reduced and corrected with an in-house software using a mix of the R statistical package and the Python programming language. The results of the U–Pb analysis were plotted with Isoplot 4.15 (Ludwig, 2008).

Seven samples were selected for Sm–Nd whole rock isotope studies. Digestion of powdered samples was done at the CPGeo in a clean room using ultra-clean reagents (HF + HNO_3 + HCl). Rare-earth elements were extracted following conventional cation exchange techniques described by Sato et al. (1995). Isotope ratios were measured with a multicollector Finnigan MAT 262 mass spectrometer and the quoted errors are given at the 2σ level. Concentrations of Sm and Nd were obtained by fused bead, acid digestion, and ICP-MS. The ^{147}Sm/^{144}Nd

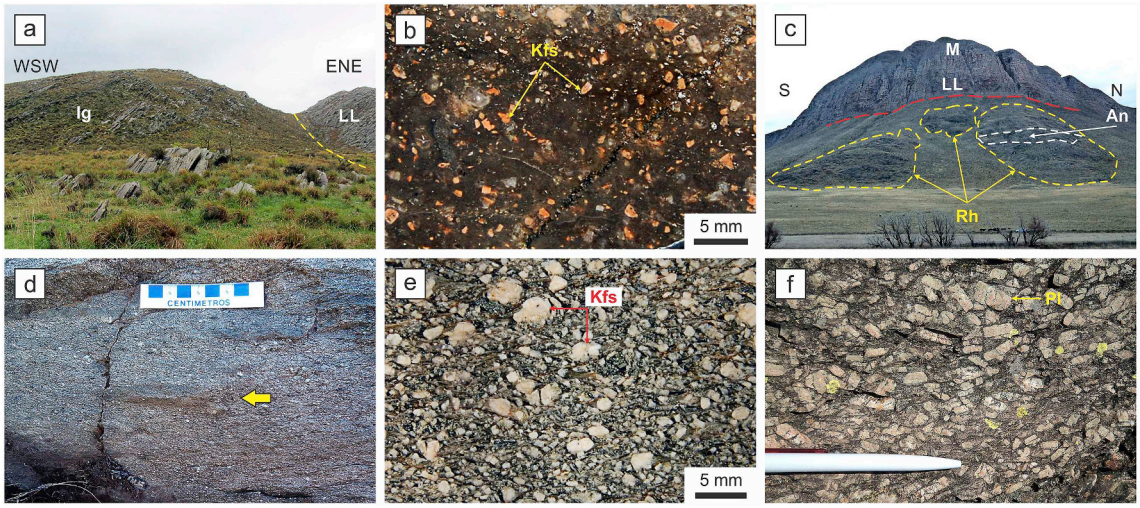

Fig. 8. a) Outcrop of the Cerro del Corral Ignimbrite (Ig). The dashed yellow line shows the tectonic contact between the ignimbrite and the La Lola Formation (LL). **b)** Polished hand sample of the Cerro del Corral Ignimbrite (phenocrysts are of K-feldspar, Kfs). **c)** Front view of the northeastern slope of Cerro Pan de Azúcar. The dashed yellow lines enclose the rhyolite (Rh) outcrops, whereas the dashed white line encloses the andesite (An) outcrop. The red dashed line marks the tectonic contact between the crystalline basement and the La Lola (LL) and Mascota (M) formations. **d)** Outcrop of the Cerro Pan de Azúcar Rhyolite in which a fiamme-like component can be seen. **e)** Polished hand sample of the Cerro Pan de Azúcar Rhyolite (phenocrysts are of K-feldspar, Kfs). **f)** Outcrop of the Cerro Pan de Azúcar Andesite (pen width = 1 cm; phenocrysts are of plagioclase, Pl). (For interpretation of the references to colour in this figure legend, the reader is referred to the Web version of this article.)

ratios were calculated using the procedures of Hamilton et al. (1983). The $^{143}Nd/^{144}Nd$ ratios were normalized to $^{146}Nd/^{144}Nd = 0.7219$ (DePaolo, 1981) and $^{143}Nd/^{144}Nd = 0.512103$ (CPGeo laboratory measurement of the JNDi-1 standard from August 2017 to August 2018). The mean value for the $^{143}Nd/^{144}Nd$ ratio of the JNDi-1 standard during the day of the analysis was 0.512102 ± 0.000004 (n = 16).

5. Petrography

As mentioned in previous sections, the SCI basement rocks are mylonitized. However, this section pays special attention to the primary igneous characteristics of these rocks.

5.1. Granitic rocks

Mylonitic granites are the most widely exposed rocks in the SCI. They crop out in Cerro del Corral (western part), Cerro 21 de Septiembre, Loma Marcelo, and Loma Meyer (Fig. 5). They are mylonitic monzogranites and syenogranites of greenish, brown, or grey colours with primary characteristics such as granular texture and medium to coarse grain size (Fig. 7a–g). In some outcrops of the Cerro del Corral Granite, the texture is porphyritic with larger crystals of K-feldspar. The most abundant minerals in these rocks are quartz, K-feldspar (microcline), plagioclase (albite-oligoclase), and biotite and/or muscovite. Accessory minerals such as garnet, zircon, apatite, and/or magnetite were observed. Secondary minerals such as epidote and calcite were also observed.

Quartz appears as subhedral to anhedral crystals of up to 2 mm in length with undulose extinction in less mylonitized rocks and as euhedral crystals of up to 40–50 μm in diameter with normal extinction and polygonal granoblastic texture in recrystallized mylonites. Quartz crystals may appear truncated by pressure solution, and then recrystallized in strain shadows. Strain fringes of fibrous sericite and calcite, together with microcrystalline quartzo-feldspathic aggregates, may link stretched and boudinaged crystals.

Microcline porphyroclasts of up to 1 cm in length exhibit core-and-mantle structure, curved cross-hatched twinning, and patches due to secondary albite exsolution, whereas plagioclase sometimes shows curved and kinked polysynthetic twinning or antiperthites in the form of parallel veins. Biotite and muscovite define the mylonitic foliation that contour quartz and feldspar crystals. Mica (especially muscovite) can also form mica fish. Garnet was only found in the Loma Meyer Granite. Crystals of this mineral are anhedral to subhedral (≤ 250 μm) and correspond to the pyrope–almandine series ($Almandine_{72.96–76.42\%}$ $Pyrope_{12.57–19.08\%}$; Appendix A).

5.2. Loma Marcelo Orthogneiss

The Loma Marcelo Granite, besides hosting the Loma Marcelo skarn, hosts an orthogneiss xenolith that crops out scarcely (< 0.5 m^2) next to the largest skarn outcrop (Fig. 7h). The orthogneiss is light brown in colour and presents incipient compositional banding (Fig. 7i). It is composed of quartz, feldspar, biotite, and garnet. Accessory minerals such as fluorite, zircon, monazite, allanite, titanite, and niobium and thorium oxides were recognized.

Quartz and feldspar (plagioclase and microcline) crystals are anhedral (≤ 3 mm) and are the most abundant minerals, denoting the granitic nature of the protolith. Biotite crystals (≤ 500 μm) constitute the fine cleavage domains of the rock, are dark reddish brown in colour, and are chloritized to a variable degree. Garnet crystals are anhedral (≤ 800 μm) and correspond to the pyrope–almandine series ($Almandine_{79.21–82.25\%}$ $Pyrope_{11.18–13.01\%}$; Appendix A). Lamellar aggregates of chlorite and anhedral crystals of epidote were observed into the fractures that cross-cut the garnet crystals and around them.

Fluorite occupies the interstices between quartz and feldspar crystals. Zircon crystals are subhedral and prismatic and have a maximum length of approximately 300 μm. The remaining accessory minerals were identified by scanning electron microscopy and X-ray dispersive energy detection. Monazite is anhedral and has a maximum length of 30 μm. Garnet and titanite contain inclusions of allanite and niobium oxide (pyrochlore?), respectively, whereas thorium oxide (thorianite?) is between quartz and feldspar in the matrix.

5.3. Cerro del Corral Ignimbrite

The Cerro del Corral Ignimbrite is mainly composed of alternating thin strips of mylonitic ignimbrites and rhyolitic ignimbrites, and minor strips of ultramylonites that look like a felsic lava. The less mylonitized

ignimbritic protolith still preserves relics of primary igneous features such as embayed and hexagonal-shaped quartz phenocrysts (≤ 2.5 mm), tabular oligoclase and microcline (≤ 2 mm) immersed in a reddish-brown to greenish-grey aphanitic matrix (Fig. 8a and b), and minor fluorite as an accessory mineral. On the basis of relict igneous phenocrysts, the ignimbrite can be classified as rhyolitic to dacitic (see also lithogeochemical features in Section 6). Additional key pyroclastic features are sub-rounded andesitic lithic fragments (1–2 mm in diameter) and glassy fragments (pumice and bubble-wall shards, < 100 μm) now devitrified and recrystallized into fine grained plumose spherulite aggregates and axiolites. Greenish-grey, lens-shaped, and flattened fiammes up to 5 cm long defining the eutaxitic texture are also devitrified and recrystallized to a quartzo-feldspathic aggregates.

In mylonitic ignimbrites, the phenocrysts are now transformed into winged objects (*e.g.*, sigma- and delta-type porphyroclasts), which preserved relics of the igneous matrix attached to them. The mylonitic matrix wraps the porphyroclasts and consists of polygonal granoblastic quartz and quartz-sericite aggregates with granolepidoblastic texture.

5.4. Cerro Pan de Azúcar Rhyolite

The mylonitized Cerro Pan de Azúcar Rhyolite exhibits highly variable crystal and clast content, from less than 10% to more than 60% (Fig. 8c–e). Scarcely fragmented quartz and feldspars are the main components, with plagioclase (albite-oligoclase) generally dominating over K-feldspar (sanidine). Crystal size is generally smaller than 6 mm in diameter. Quartz is generally hexagonal, with frequent embayed outlines. Feldspars show simple (sanidine) and polysynthetic (plagioclase) twinning, are euhedral to subhedral and are replaced by clay minerals, sericite, and minor epidote. On the basis of relict igneous phenocrysts, the rock can be classified as dacitic to rhyolitic (see also lithogeochemical features in Section 6). Lithic fragments and fiamme-like components are scarcer than in the Cerro del Corral Ignimbrite, and up to a few centimetres in length. They are immersed in a pale grey microcrystalline matrix. Lithic fragments are heterogeneously distributed and show textures such as microfelsitic, spherulitic, porphyritic, and trachytic. Additionally, lithic fragments with fine-grained granular texture denoting plutonic origin are rarely found. Fiamme-like components are wispy and elongated domains devitrified into spherulitic and clean quartzo-feldspathic aggregates (Fig. 8d). Due to the above described primary volcanic features, we interpret the Cerro Pan de Azúcar Rhyolite (or Dacite) as another ignimbrite outcrop.

The microcrystalline matrix consists of heterogeneous aggregates of quartz and feldspar. It is altered to sericite and quartz and shows mylonitic foliation. Partly, the matrix has micropoikilitic texture, or is micropoikilitically devitrified in the surrounding of the larger crystals. Plumose, bow-tie, and spherical spherulitic devitrification is also observed, although no relict shard or pumice clasts could be identified. Sericite-rich bands with scarce biotite, epidote, and calcite define the mylonitic foliation.

5.5. Cerro Pan de Azúcar Andesite

The Cerro Pan de Azúcar Rhyolite is cut by an 80 m long and 30 m wide andesitic body (Fig. 8c). Like its host rock, the andesite is mylonitized and its contact with the rhyolite is sharp and parallel to the mylonitic foliation. No presence of chilled margins was observed. The andesite has a porphyritic texture with large phenocrysts of greyish-white plagioclase immersed in a dark green aphanitic groundmass with vesicular and amygdaloidal structures (Fig. 8f). The phenocrysts and plagioclase crystals of the groundmass ($An_{5–20}$) reach maximum lengths of 4 cm and 500 μm, respectively; they are euhedral to subhedral and epidotized to variable degrees. The plagioclase crystals of the groundmass define a pilotaxitic texture. The plagioclase composition of the Cerro Pan de Azúcar Andesite is less calcic than the composition of common andesites ($An_{40–50}$; Best, 2003).

Epidote is common as an alteration mineral in the phenocrysts, interstitially in the groundmass, and filling vesicles and fractures together with quartz and calcite. Sericite and chlorite sheets define the mylonitic foliation. Along the foliation planes, epidote, actinolite, quartz, and Fe-Mn oxides were also identified.

Along the outcrop, a certain orientation of the plagioclase phenocrysts coinciding with the direction of the mylonitic foliation can be observed, as well as a decrease in the grain size of the phenocrysts from the core of the andesitic body to the contact with the hosting rhyolite. These are typical characteristics of dykes.

6. Lithogeochemistry

Major and trace elements were determined in plutonic and volcanic rock samples from the SCI. Samples were taken from sparsely deformed zones. The complete results of the analysed samples are presented in Appendix B.

6.1. Plutonic rocks

The mylonitic granites plot within the granite field of the Ab-An-Or diagram of Barker (1979) (Fig. 9a). This diagram, based on the normative composition of the rock, can also be used with deformed and metamorphosed granitic rocks, allowing the original type of magma to be estimated.

The analysed rocks plot within de subalkaline and high-K calc-alkaline fields of the SiO_2 vs. $Na_2O + K_2O$ (Irvine and Baragar, 1971) and SiO_2 vs. K_2O (Peccerillo and Taylor, 1976) diagrams, respectively. However, the Loma Marcelo Orthogneiss has fluorite and pyrochlore (?), common accessory minerals of alkaline rocks.

Regarding the alumina saturation, the mylonitic granites plot within the peraluminous field of the Al/(Ca + Na + K) vs. Al/(Na + K) diagram of Shand (1927) (Fig. 9c). The peraluminous affinity of these rocks is further supported by the presence of major minerals such as biotite + muscovite and/or accessory minerals such as garnet. The epidote, widely distributed in the SCI basement rocks, would be a product of the superimposed metamorphism. In the analysed rocks, the alumina saturation index [ASI = molar $Al_2O_3/(CaO + Na_2O + K_2O)$] is between 1.01 and 1.48, whereas normative corundum values are mainly between 1.16 and 5.50%.

In the primitive mantle-normalized spidergrams, the mylonitic granites exhibit a marked enrichment in incompatible elements with respect to the most compatible elements, as well as negative anomalies of Nb, Ta, Sr, P, and/or Ti (Fig. 10a). The mantle-normalized patterns of the mylonitic granites are similar to each other; however, the Loma Marcelo Granite has a somewhat lower content of trace elements. The Loma Marcelo Orthogneiss is enriched in high field strength elements (HFSE), except Eu and Ti, and something depleted in Ba, Sr, and P (Fig. 10a).

The total rare-earth elements (REE) content of the mylonitic granites vary between 72.83 and 300.54 ppm. In the chondrite-normalized spidergrams, these rocks exhibit a marked enrichment in light rare-earth elements (LREE) with respect to the heavy rare-earth elements (HREE) (La_N/Lu_N = 7.31–103.28) (Fig. 10c). Eu anomalies are usually negative (Eu/Eu* = 0.37–0.51), except in the Loma Marcelo Granite that has positive Eu anomalies (Eu/Eu* = 2.37–2.55). Negative Eu anomalies indicate fractionation of plagioclase at the source. On the other hand, the observed positive Eu anomalies could be the result of plagioclase crystallization from a liquid relatively impoverished in Eu due to prior fractionation of this element at the source (*e.g.*, Korhonen et al., 2010). Plagioclase formed under these conditions has low Eu contents and its accumulation is characterized by the presence of positive anomalies of this element.

The total REE content of the Loma Marcelo Orthogneiss varies between 201.00 and 236.80 ppm. Chondrite-normalized REE patterns exhibit marked negative Eu anomalies (Eu/Eu* = 0.17–0.20)

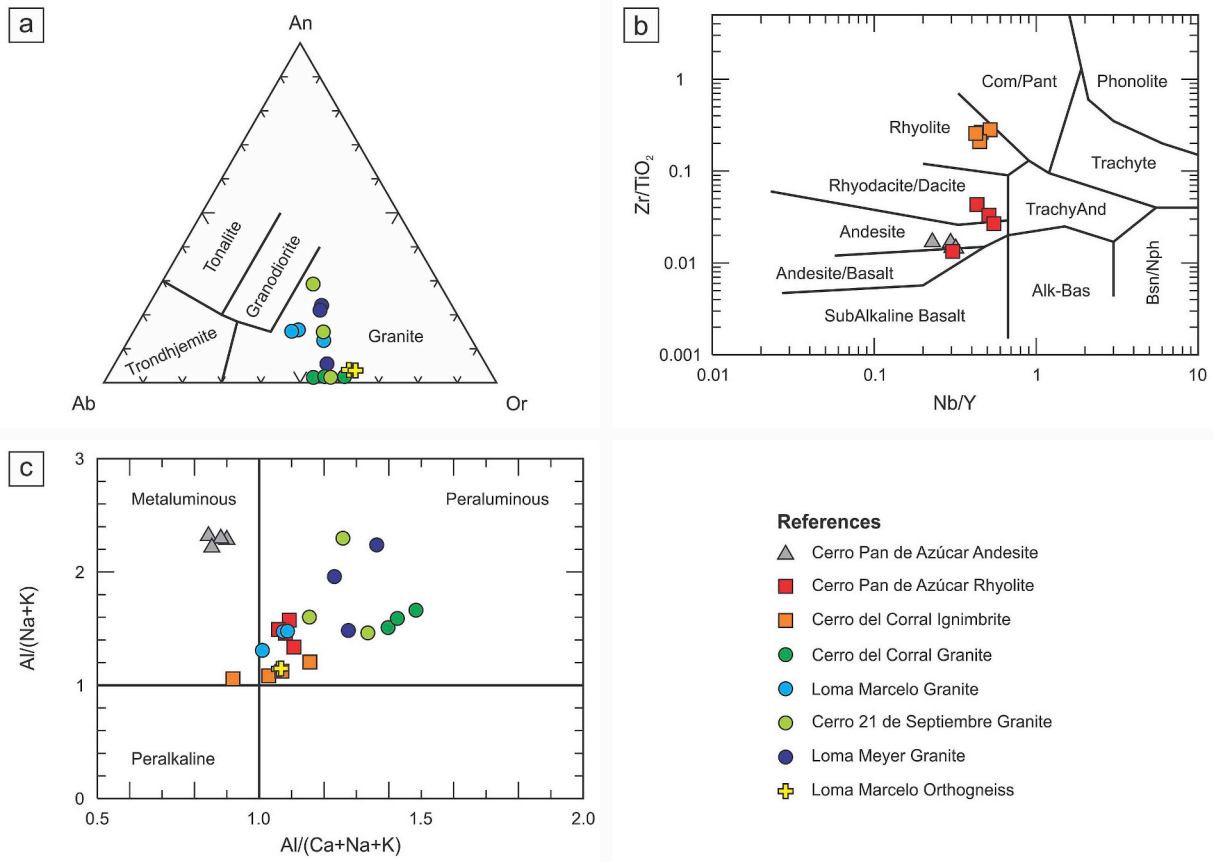

Fig. 9. Rock classification diagrams for the Sauce Chico Inlier basement rocks. **a)** Ab-An-Or diagram (Barker, 1979) for plutonic rock samples. **b)** Nb/Y vs. Zr/TiO_2 diagram (Winchester and Floyd, 1977) for volcanic rock samples. **c)** Alumina saturation diagram of Shand (1927).

(Fig. 10c). The depletion in LREE with respect to the HREE (La_N/Lu_N = 6.96–7.04) and the positive slope of the HREE pattern (Tb_N/Lu_N = 0.69–0.71) would be a consequence of the presence of garnet in this rock, mineral that is characterized by concentrating the HREE during its formation. Accessory minerals such as zircon, allanite, monazite, and Nb and Th oxides would also be controlling the content of REE, U, and Th of the Loma Marcelo Orthogneiss due to the capability of such minerals to concentrate these elements.

When plotted in tectonic discrimination diagrams, the mylonitic granites plot within the A- and I&S-type fields of the Ga/Al vs. Zr diagram of Whalen et al. (1987) (Fig. 11a). The Yb-Ta diagram of Pearce et al. (1984) allows better discrimination of the mylonitic granites (Fig. 11b). In this last diagram, the mylonitic granites plot mainly within the volcanic arc granites (VAG) field, whereas the Loma Marcelo Orthogneiss plots into the within-plate granites (WPG) field. In relation to the orthogneiss, the high Ga/Al and FeO_T/MgO ratios, the low Zr/Nb ratio, the HFSE content (*e.g.*, Y, Nb, Ta, U, Th), and the presence of fluorite are diagnostic of A-type granites and, usually, of acid within-plate magmatism (Pearce et al., 1984; Leat et al., 1986; Whalen et al., 1987; Eby, 1990). In the Y-Nb-3Ga diagram of Eby (1992), the Loma Marcelo Orthogneiss plots within the A_1 field (Fig. 11c), which is associated with magmas derived from similar sources to those of ocean island basalts (OIB) and emplaced during intraplate magmatism (*e.g.*, continental rifting).

6.2. Volcanic rocks

6.2.1. Cerro del Corral Ignimbrite and Cerro Pan de Azúcar Rhyolite

The Cerro del Corral Ignimbrite and the Cerro Pan de Azúcar Rhyolite plot within the rhyolite and rhyodacite/dacite fields, respectively, of the Nb/Y vs. Zr/TiO_2 diagram (Winchester and Floyd, 1977) (Fig. 9b). All samples plot within the subalkaline and high-K calc-alkaline fields of the SiO_2 vs. $Na_2O + K_2O$ (Irvine and Baragar, 1971) and SiO_2 vs. K_2O (Peccerillo and Taylor, 1976), respectively, suggesting that both units would be part of subalkaline volcanic suites. However, the high Ga/Al and FeO_T/MgO ratios, the low Zr/Nb ratio, the relatively high content of some HFSE (*e.g.*, Y, U, Th), and the presence of fluorite indicate an alkaline geochemical signature for the Cerro del Corral Ignimbrite (Pearce et al., 1984; Leat et al., 1986; Whalen et al., 1987; Eby, 1990). Both volcanic units plot within the peraluminous field of the alumina saturation diagram of Shand (1927) (Fig. 9c). The alumina saturation index (ASI) is between 0.92 and 1.16, whereas normative corundum values are between 0.39 and 1.97%.

Primitive mantle-normalized spidergrams of the Cerro del Corral Ignimbrite and the Cerro Pan de Azúcar Rhyolite exhibit enrichment in incompatible elements with respect to the most compatible elements (Fig. 10b). The rhyolite is clearly distinguished from the ignimbrite due to the presence of positive anomalies of Ba, U, Nb, and Pr and negative anomalies of Th, P, Nd, Ti, and Dy.

The total REE content of the Cerro del Corral Ignimbrite varies between 143.53 and 176.93 ppm. Chondrite-normalized REE patterns exhibit a little enrichment in LREE with respect to the HREE (La_N/Lu_N = 1.33–1.70) and marked negative Eu anomalies (Eu/Eu^* = 0.02–0.04) (Fig. 10d). The extreme fractionation of feldspar could be responsible for the marked negative Eu anomalies. On the other hand, the total REE content of the Cerro Pan de Azúcar Rhyolite varies between 95.10 and 174.01 ppm. Chondrite-normalized REE patterns exhibit a greater enrichment in LREE with respect to the HREE (La_N/Lu_N = 8.04–15.66) and a less marked negative Eu anomalies (Eu/Eu^* = 0.52–0.78) (Fig. 10d).

In the Ga/Al vs. Zr (Whalen et al., 1987) and Yb-Ta (Pearce et al., 1984) tectonic discrimination diagrams, the Cerro del Corral Ignimbrite

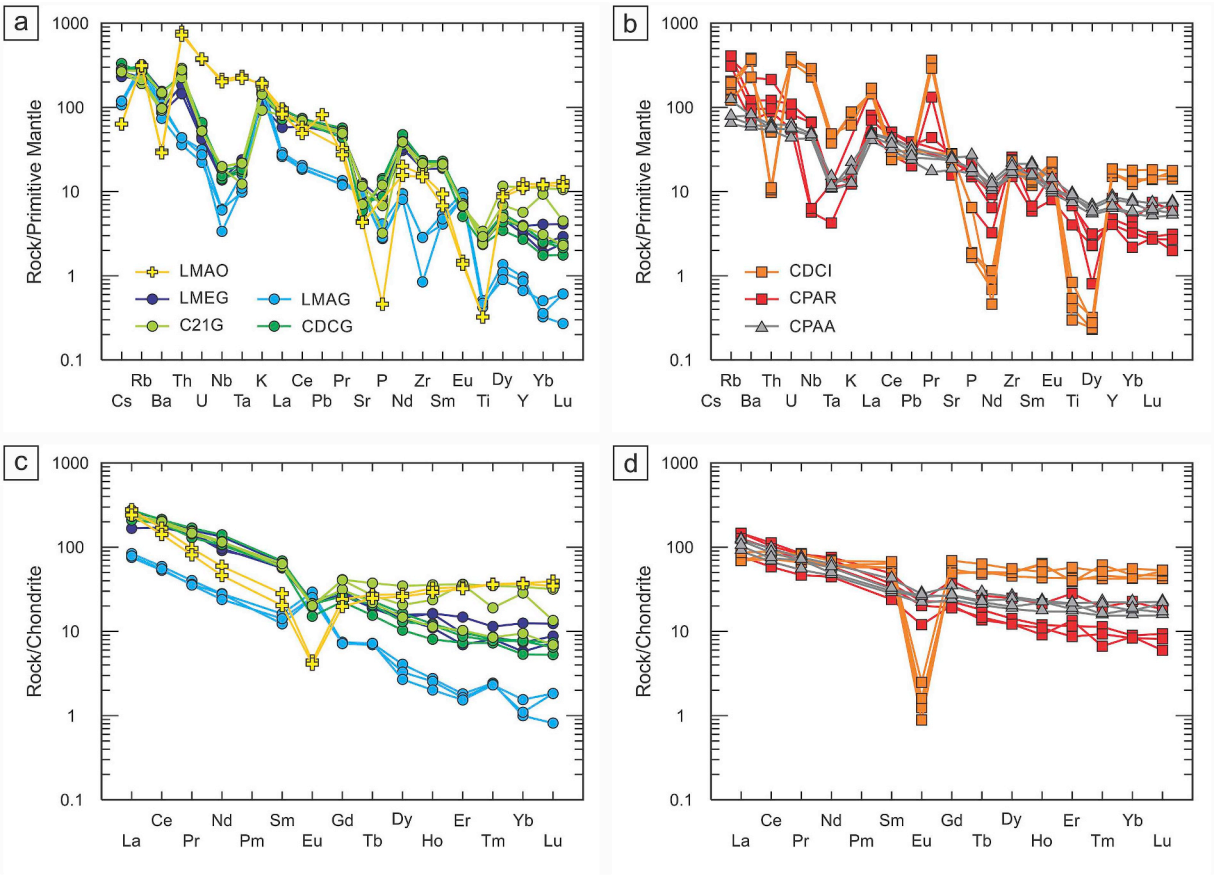

Fig. 10. Multi-element diagrams for the Sauce Chico Inlier basement rocks. Trace element diagram normalized to primitive mantle values (Sun and McDonough, 1989) for plutonic (a) and volcanic (b) rock samples. Figures c and d show REE diagrams normalized to chondrite values (McDonough and Sun, 1995) for plutonic and volcanic rock samples, respectively. **Abbreviations:** LMEG = Loma Meyer Granite, LMAO = Loma Marcelo Orthogneiss, C21G = Cerro 21 de Septiembre Granite, LMAG = Loma Marcelo Granite, CDCG = Cerro del Corral Granite, CDCI = Cerro del Corral Ignimbrite, CPAR = Cerro Pan de Azúcar Rhyolite, CPAA = Cerro Pan de Azúcar Andesite.

and the Cerro Pan de Azúcar Rhyolite are clearly distinguishable from each other (Fig. 10a and b). The first one plots within the A-type and within-plate granites (WPG) fields and the second one plots within the I &S-type and volcanic arc granites (VAG) fields. Additionally, the Cerro del Corral Ignimbrite plots within the A_2 field of the Y-Nb-3Ga diagram (Eby, 1992) (Fig. 10c). Unlike A_1-type magmas, A_2-type magmatism derives from a continental crust that has been affected by continental recycling (Eby, 1992).

6.2.2. *Cerro Pan de Azúcar Andesite*

The Cerro Pan de Azúcar Andesite plots within the andesite field of the Nb/Y vs. Zr/TiO_2 diagram (Winchester and Floyd, 1977) (Fig. 9b), the subalkaline field of the SiO_2 vs. $Na_2O + K_2O$ diagram (Irvine and Baragar, 1971), and the metaluminous field of the alumina saturation diagram of Shand (1927) (Fig. 9c). The alumina saturation index (ASI) is between 0.84 and 0.90. It does not present normative quartz or corundum, but it has normative olivine and diopside.

Primitive mantle-normalized spidergram shows enrichment in incompatible elements with respect to the most compatible elements, as well as marked negative anomalies of Ta and K and other less negative anomalies of Nd (Fig. 10b). Lithogeochemical results also show enrichment in some large-ion lithophile elements (*e.g.*, Sr, Ba). The REE content is low (110.79–155.38 ppm). Chondrite-normalized spidergram shows enrichment in LREE with respect to the HREE (La_N/Lu_N = 5.49–6.14) and slightly negative Eu anomalies (Eu/Eu^* = 0.73–0.91) (Fig. 10d).

The Cerro Pan de Azúcar Andesite plots within the calc-alkali field (C) of the Zr-Ti/100-3Y diagram of Pearce and Cann (1973) (Fig. 11d) and the arc-basalts field (D) of the Th-Hf/3-Nb/16 diagram of Wood (1980) (Fig. 11e). The "D" field of this last diagram can be subdivided into islands arc tholeiites (Hf/Th > 3) and calc-alkaline basalts (Hf/Th < 3). The Hf/Th ratios between 1.15 and 1.27 locate the Cerro Pan de Azúcar Andesite within the calc-alkaline basalts field of the Th-Hf-Nb diagram, reinforcing what the Zr-Ti-Y diagram indicates.

7. LA-ICP-MS U–Pb zircon dating

Six new LA-ICP-MS U–Pb zircon crystallization ages were obtained for the SCI igneous rocks (Fig. 4). Results with discordances < 10% were selected for magmatic crystallization age determination. Ages are reported and plotted at the 2σ level. For zircon grains with ages above 1.0 Ga the $^{207}Pb/^{235}U$ age was preferred, whereas for zircon grains with ages less than 1.0 Ga the $^{206}Pb/^{238}U$ age was chosen. It was not possible to separate zircon grains from the Cerro Pan de Azúcar Andesite. The complete results of the analysed samples are presented in Appendix C.

7.1. *Loma Meyer granite (sample LMEG-1)*

Thirty-three zircon grains from the Loma Meyer Granite were analysed. The zircon grains are mainly prismatic dipyramidal with light brown colours. Some grains have well-marked pyramidal terminations, whereas others have somewhat sub-rounded ends. The average zircon size is 150 × 70 μm. Under CL, zircon grains have central cores and rims with magmatic oscillatory zoning (Fig. 12a). The best estimate U–Pb concordia age for the crystallization of the Loma Meyer Granite (12 spots) is 783.8 ± 3.7 Ma with MSWD = 0.99 (Fig. 12b). Ages

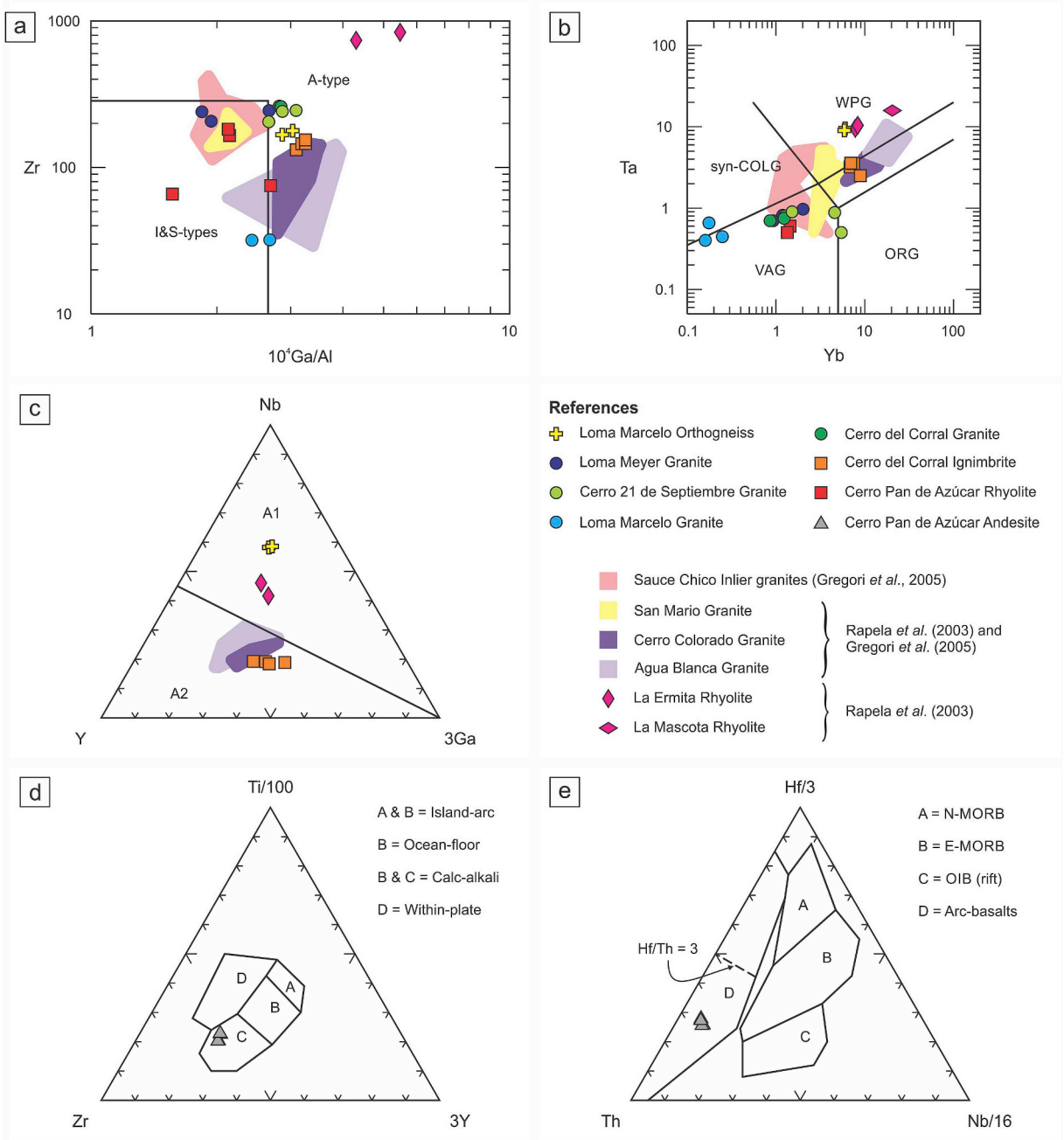

Fig. 11. Tectonic discrimination diagrams for the Sauce Chico Inlier basement rocks. Granitic and rhyolitic rocks: **a)** Ga/Al vs. Zr of Whalen et al. (1987); **b)** Yb vs. Ta of Pearce et al. (1984); **c)** Y-Nb-Ga of Eby (1992) for discrimination of A-type rocks. Cerro Pan de Azúcar Andesite: **d)** Ti-Zr-Y of Pearce and Cann (1973); **e)** Hf-Th-Nb of Wood (1980). **Abbreviations:** WPG = within-plate granites, VAG = volcanic arc granites, syn-COLG = syn-collision granites, ORG = ocean-ridge granites, N-MORB = normal mid-ocean ridge basalts, E-MORB = enriched mid-ocean ridge basalts, OIB = ocean island basalts.

between *ca.* 1894 and 821 Ma are interpreted as inheritance. It should be noted that all of them are discordant (Fig. 12b). Ages between *ca.* 767 and 658 Ma were not considered in the calculations.

7.2. Loma Marcelo Orthogneiss (sample LMAO-2)

Twenty-two zircons were analysed from the Loma Marcelo Orthogneiss, a xenolith hosted in the Loma Marcelo Granite (Fig. 5). Zircon grains are stubby dipyramidal prisms with light brown colour. The lengths and widths of the zircon grains are 120–320 μm and 50–100 μm, respectively. The analysed zircon grains are of magmatic origin as indicated by their euhedral shapes and oscillatory zoning under CL (Fig. 12c); some of them are metamictic. The best estimate U–Pb concordia age for the crystallization of the Loma Marcelo Orthogneiss (5 spots) is 776.5 ± 4.7 Ma with MSWD = 5.0 (Fig. 12d). Ages between *ca.* 809 and 792 Ma are interpreted as inheritance. On the other hand, ages between *ca.* 755 and 457 Ma were not considered in the calculations. Some of the latter, at least the younger ones, are interpreted as the result of Pb loss. Worth highlighting the presence of zircon rims with concordant ages of 630.6 ± 4.4 Ma and 640.9 ± 4.5 Ma. One spot was discarded due to analytical problems.

7.3. Cerro 21 de Septiembre Granite (sample C21G-1)

Twenty-four zircon grains from the Cerro 21 de Septiembre Granite were analysed. The zircon grains are prismatic dipyramidal with light

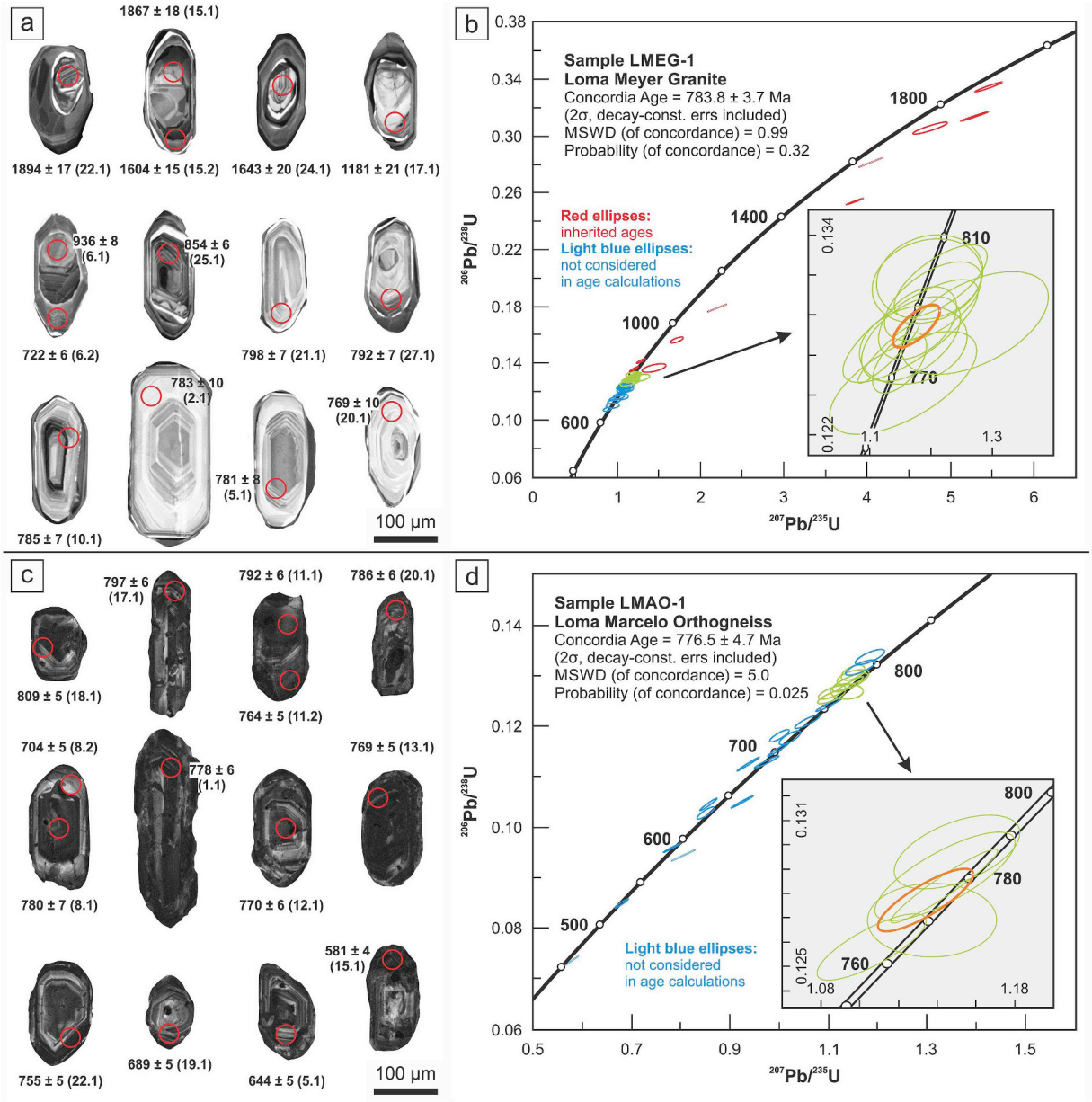

Fig. 12. Cathodoluminescence images of some analysed zircons and concordia diagrams for the Loma Meyer Granite (a–b) and for the Loma Marcelo Orthogneiss (c–d). Orange ellipses correspond to the concordia ages. (For interpretation of the references to colour in this figure legend, the reader is referred to the Web version of this article.)

brown colours, have an average size of 185 × 75 µm, and show magmatic oscillatory zoning under CL (Fig. 13a). The best estimate U–Pb concordia age for the crystallization of the Cerro 21 de Septiembre Granite (12 spots) is 620.8 ± 5.8 Ma with MSWD = 1.5 (Fig. 13b). Ages between *ca.* 1991 and 769 Ma are interpreted as inheritance. Two ages of *ca.* 596 Ma and *ca.* 599 Ma were not considered in the calculations.

7.4. Loma Marcelo Granite (sample LMAG-2)

Twenty-one zircons were analysed from the Loma Marcelo Granite. Zircon grains are mostly prismatic and stubby with varied shades of brown in colour; some grains are broken. The lengths and widths of the zircon grains are 110–262 µm and 50–160 µm, respectively. The analysed zircon grains are of magmatic origin as indicated by their euhedral shapes and oscillatory zoning under CL (Fig. 13c). Some grains are dark grey with no internal structure under CL due to metamictization. A few of them show large metamictic cores that have expanded and cracked the rims. Despite metamictization, the analysed spots are homogeneous in terms of the obtained ages and show little dispersion of the Th/U ratios (Appendix C). The best estimate U–Pb concordia age for the crystallization of the Loma Marcelo Granite (14 spots) is 620.3 ± 2.5 Ma with MSWD = 3.2 (Fig. 13d). This concordia age is identical to that of 621.6 ± 2.2 Ma (MSWD = 0.31) obtained for the same unit by Ballivián Justiniano et al. (2019). Ages between *ca.* 642 and 630 Ma are interpreted as inheritance. Worth highlighting the presence of two zircon cores with concordant ages of 632.6 ± 4.9 Ma and 635.5 ± 4.5 Ma and one zircon rim with a concordant age of 630.2 ± 4.7 Ma. Ages between *ca.* 611 and 589 Ma were not considered in the calculations.

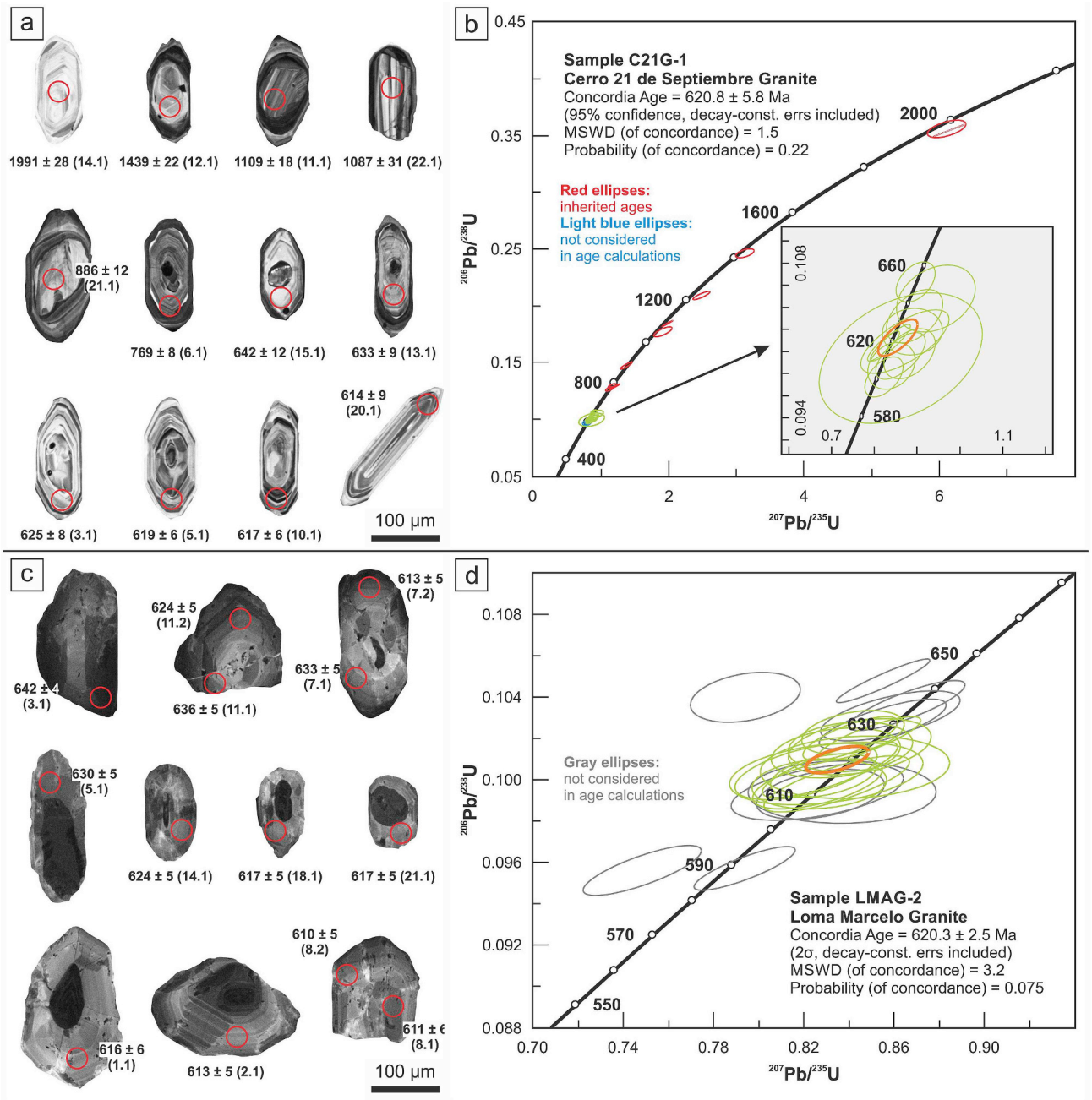

Fig. 13. Cathodoluminescence images of some analysed zircons and concordia diagrams for the Cerro 21 de Septiembre Granite (a–b) and for the Loma Marcelo Granite (c–d). Orange ellipses correspond to the concordia ages. (For interpretation of the references to colour in this figure legend, the reader is referred to the Web version of this article.)

7.5. Cerro del Corral Ignimbrite (sample CDCI-4)

Nineteen zircon grains from the Cerro del Corral Ignimbrite were analysed. The zircon grains are mainly prismatic, both long and short, with varied shades of brown in colour. The grains usually show well-developed pyramidal terminations. The lengths and widths of the zircon grains are 95–270 µm and 50–120 µm, respectively. Under CL, zircon grains show magmatic oscillatory zoning or do not show any internal structure (Fig. 14a); in both cases, zircon grains can be dark grey due to metamictization. The best estimate U–Pb concordia age for the crystallization of the Cerro del Corral Ignimbrite (7 spots) is 577.3 ± 3.9 Ma with MSWD = 3.6 (Fig. 14b). Ages of *ca.* 601–588 Ma and *ca.* 512 Ma were not considered in the calculations. Seven spots were discarded due to their high contents of common Pb.

7.6. Cerro Pan de Azúcar Rhyolite (sample CPAR-3)

Twenty-four zircons were analysed from the Cerro Pan de Azúcar Rhyolite. Zircon grains are mostly prismatic dipyramidal with light brown colours to colourless. The lengths and widths of the zircon grains are 120–225 µm and 40–75 µm, respectively. The analysed zircon grains are of magmatic origin as indicated by their euhedral shapes and oscillatory zoning under CL (Fig. 14c). In the Cerro Pan de Azúcar Rhyolite, two zircon populations define concordia ages of 567.2 ± 4.7 Ma (13 spots; MSWD = 0.0012) and 543.6 ± 4.0 Ma (7 spots; MSWD = 2.7) (Fig. 14d). There are no differences in the location of the spots or in the Th/U ratios (Appendix C), so the oldest concordia age could be interpreted as corresponding to a previous eruptive event. The younger age would correspond to the crystallization age of the

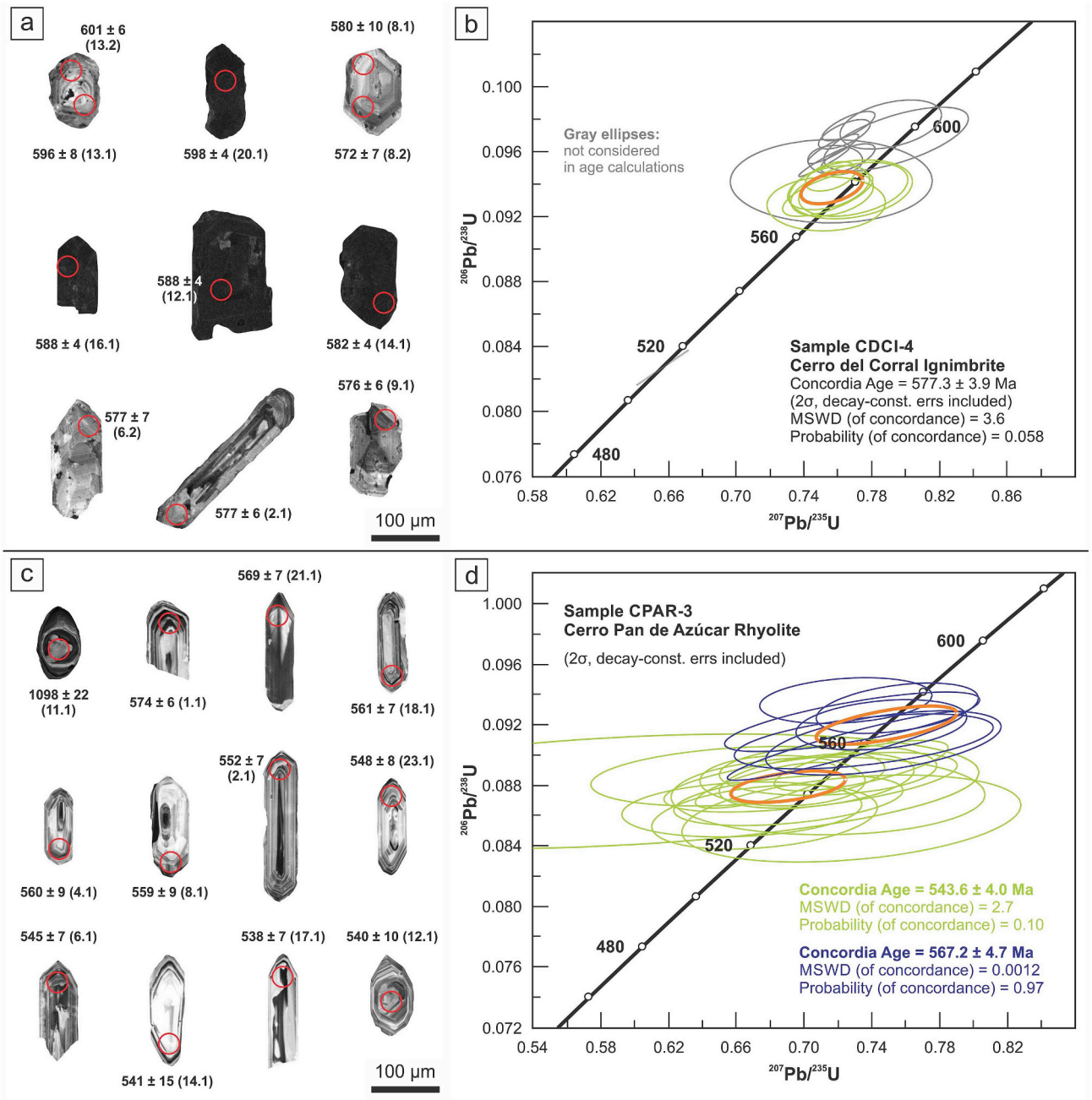

Fig. 14. Cathodoluminescence images of some analysed zircons and concordia diagrams for the Cerro del Corral Ignimbrite (a–b) and for the Cerro Pan de Azúcar Rhyolite (c–d). Orange ellipses correspond to the concordia ages. (For interpretation of the references to colour in this figure legend, the reader is referred to the Web version of this article.)

rhyolite. An age of *ca.* 1098 Ma is interpreted as inheritance. Three ages between *ca.* 520 and 516 Ma were not considered in the calculations.

8. Sm–Nd isotope data

Nd isotope ratios were determined in seven selected samples of the SCI igneous rocks (Table 1). Isotopic ratios were determined in sparsely deformed rock samples, with the exception of sample 19198, which corresponds to a much foliated mylonitic granite (Loma Marcelo Granite; whole rock geochemistry and U–Pb geochronology of this sample can be found in Ballivián Justiniano et al. (2017) and Ballivián Justiniano et al. (2019), respectively). Table 1 also includes the isotopic ratios determined by Rapela et al. (2003) for the Cerro del Corral Granite and Ignimbrite. The εNd diagram for igneous rocks of the SCI is shown in Fig. 15. The Sr isotope ratios were not determined due to the high mobility of Rb and Sr during tectono-metamorphic events, mainly when the fluid circulation was high (Grecco et al., 2000; Ballivián Justiniano et al., 2017, 2019). Rapela et al. (2003) indicated meaningless initial $^{87}Sr/^{86}Sr$ ratios calculated for several samples of the Ventania System basement.

Tonian rocks not only show differences in their lithogeochemical composition but also in their Nd isotope ratios. The Loma Meyer Granite has an εNd_{784} of −7.20, denoting an important crustal component. On the other hand, the Loma Marcelo Orthogneiss has an εNd_{777} of +1.65, indicating an input of juvenile material. Regarding the Ediacaran rocks, they show an increase in the $\varepsilon Nd_{(t)}$ values, from −9.94 to −3.38, as the crystallization age decreases.

Nd model ages (T_{DM}) of the SCI basement rocks are between 1.80

Table 1
Sm–Nd whole rock isotope data for samples from the Sauce Chico Inlier basement.

Sample	Unit	Age (Ma)	Sm (ppm)	Nd (ppm)	$^{147}Sm/^{144}Nd$	$^{143}Nd/^{144}Nd$	Error (2σ)	$(^{143}Nd/^{144}Nd)_i$	$\varepsilon Nd_{(0)}$ [b]	$\varepsilon Nd_{(t)}$ [c]	T_{DM} [d] (Ga)	T_{DM} [e] (Ga)
LMEG-1	Loma Meyer Granite	784	9.63	60.8	0.095761	0.511751	0.000004	0.511259	−17.31	−7.20	1.73	
LMAO-2	Loma Marcelo Orthogneiss	777	3.00	21.0	0.086371	0.512161	0.000004	0.511721	−9.31	+1.65	1.14	
C21G-1	Cerro 21 de Septiembre Granite	621	8.67	53.3	0.098347	0.511729	0.000005	0.511329	−17.73	−9.94	1.79	
LMAG-2	Loma Marcelo Granite	620	2.09	10.9	0.086643	0.511703	0.000005	0.511351	−18.24	−9.53	1.66	
19198	Loma Marcelo Granite	622	4.93	32.0	0.093146	0.511260	0.000004	0.510881	−26.87	−18.67	2.28	
SLV005[a]	Cerro del Corral Granite	607	8.76	50.5	0.104900	0.511803	0.003% (1σ)	0.511386	−16.29	−9.18	1.80	
CDCI-4	Cerro del Corral Ignimbrite	577	9.91	31.4	0.190815	0.512294	0.000004	0.511572	−6.71	−6.29	4.58	1.73
SLV006[a]	Cerro del Corral Ignimbrite	577	8.55	25.9	0.199700	0.512307	0.003% (1σ)	0.511552	−6.46	−6.69	6.54	1.76
CPAR-3	Cerro Pan de Azúcar Rhyolite	544	5.39	32.3	0.100891	0.512124	0.000005	0.511764	−10.03	−3.38	1.32	

d & e = calculated using a "$(^{147}Sm/^{144}Nd)_{DM,\ today}$" value of 0.219 and a "$(^{143}Nd/^{144}Nd)_{DM,\ today}$" value of 0.513151 (Liew and Hofmann, 1988).
[a] Data from Rapela et al. (2003) (the values of εNd and T_{DM} were calculated using the ratios and models listed below).
[b] Calculated using a "$(^{143}Nd/^{144}Nd)_{CHUR,\ today}$" value of 0.512638 (Goldstein et al., 1984).
[c] Calculated using a "$(^{147}Sm/^{144}Nd)_{CHUR,\ today}$" value of 0.1967 (Peucat et al., 1989) and a "$(^{143}Nd/^{144}Nd)_{CHUR,\ today}$" value of 0.512638 (Goldstein et al., 1984).
[d] Calculated following model of DePaolo (1981).
[e] Calculated following two-stage model of Liew and Hofmann (1988).

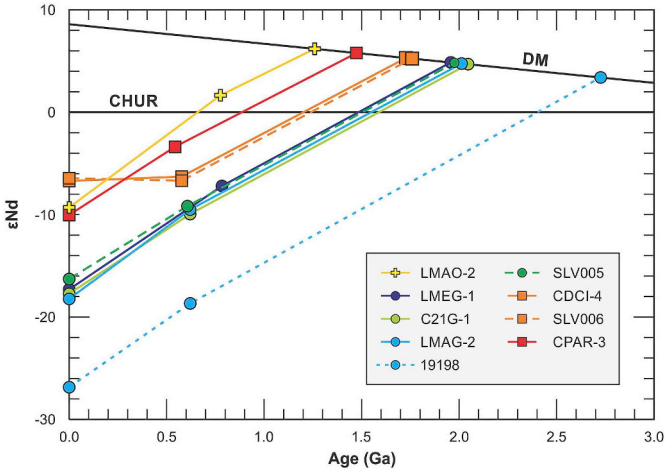

Fig. 15. εNd diagram for the Sauce Chico Inlier basement rocks (Rapela et al., 2003; this work). Mantle separation ages with an intermediate crustal stage (T_{DM}^{e} in Table 1) were calculated when incoherent values for direct mantle separation ages (T_{DM}^{d} in Table 1) were obtained.

and 1.14 Ga. These ages may result from the mixing of older crust (Mesoproterozoic, Palaeoproterozoic, or even older) with juvenile material of Neoproterozoic age. It should be noted that the Loma Meyer and Cerro 21 de Septiembre granites contain Palaeoproterozoic and Mesoproterozoic inherited ages. In the case of the Ediacaran magmatism, even reworking of Tonian rocks might contribute as well. This seems to be plausible due to the presence of xenoliths of Tonian rocks (*e.g.*, Loma Marcelo Orthogneiss) hosted in Ediacaran rocks (*e.g.*, Loma Marcelo Granite). The geochronological and isotopic results would suggest different contributions of juvenile and reworked older crust, which may lead to the different Sm–Nd signatures recorded in the SCI basement rocks. This means that the model ages of the SCI basement rocks cannot be interpreted as the age of the reworked crust. In addition, based on the different inherited ages, a metasedimentary source as the reworked component could be considered (*e.g.*, metapelite xenoliths hosted in the Loma Meyer and Cerro 21 de Septiembre granites).

Sample 19198 is an intensely deformed granite from Loma Marcelo. Compared with a much less deformed sample of the same unit (sample LMAG-2), sample 19198 presents a more negative εNd_{622} of −18.67 and an older model age of 2.28 Ga. This fact is interpreted as the result of a large component of a reworked crust.

The relatively similar values of $\varepsilon Nd_{(t)}$ obtained in this work and by Rapela et al. (2003) for the SCI basement rocks suggest that the Nd isotope ratios were not disturbed despite deformation and metamorphism. The great circulation of fluids and the intense deformation that opened the system for the major and trace elements (von Gosen et al., 1990; Grecco et al., 2000; Ballivián Justiniano et al., 2019) did not rehomogenize the Nd isotopic system. If this occurred, one would expect a large disparity in the isotope ratios of $^{147}Sm/^{144}Nd$ and $^{143}Nd/^{144}Nd$ and in the values of $\varepsilon Nd_{(t)}$ of the analysed samples. However, it did not happen.

Rapela et al. (2003) pointed out that the partial melting of the Palaeoproterozoic rocks of the Tandilia System would be the most likely origin for the Cerro del Corral Granite. In this sense, we found six Palaeoproterozoic concordant inherited ages between *ca.* 1996 and 1643 Ma, eleven concordant inherited ages between *ca.* 1439 and 792 Ma, and few concordant inherited ages between *ca.* 641 and 630 Ma. Some inherited ages are discordant (*e.g.*, Loma Meyer Granite, with $^{207}Pb/^{206}Pb$ ages between 1111 ± 138 Ma and 1931 ± 36 Ma), so their isotopic systematics could be disturbed and then they probably represent older zircons.

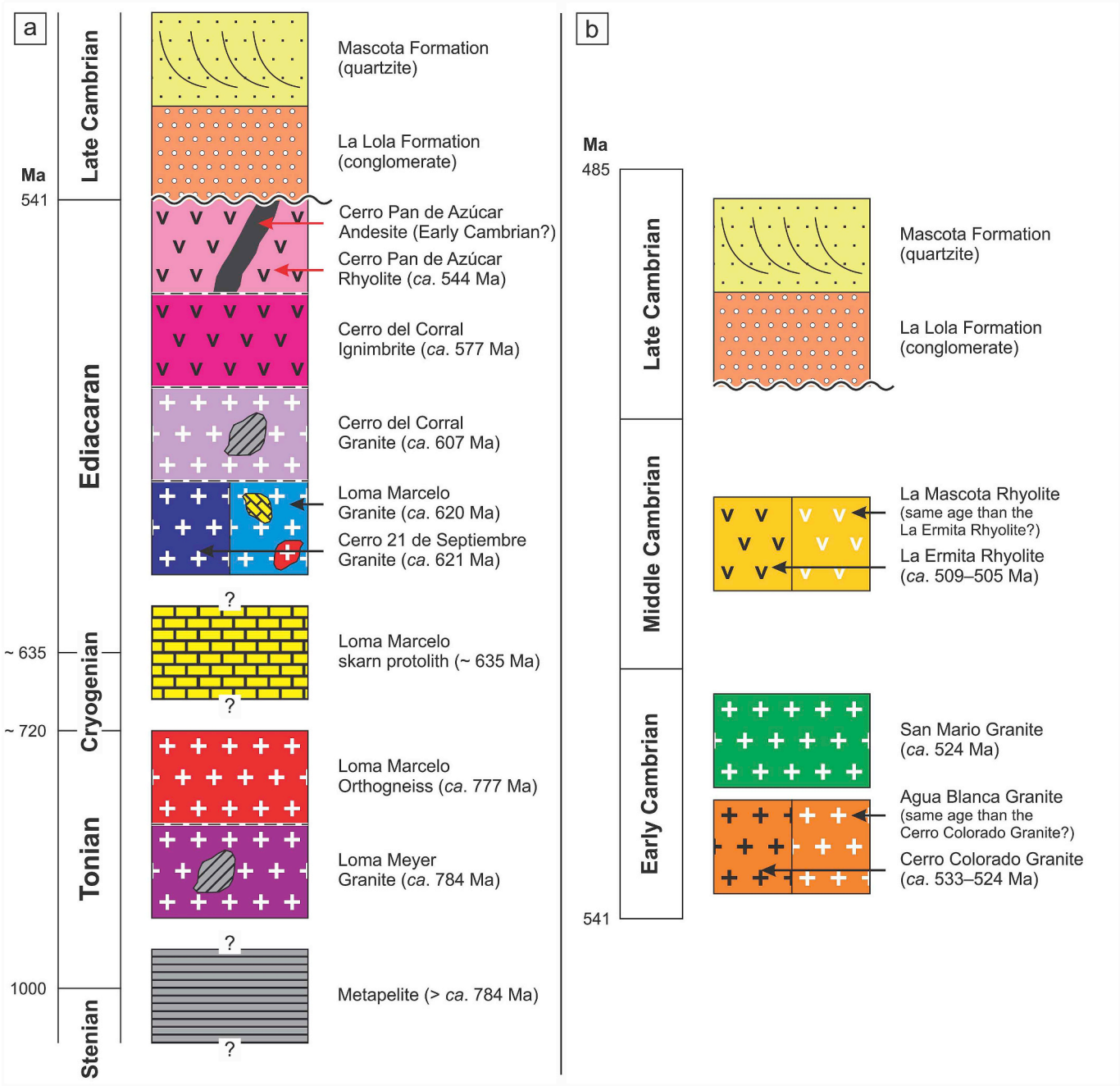

Fig. 16. Stratigraphic column of the Sauce Chico Complex inside (a) and outside (b) the Sauce Chico Inlier. See Fig. 3 for the regional geological setting.

9. Discussion

9.1. Evolution of the Ventania System basement

U–Pb age variations indicate a complex magmatic history for the SCI basement rocks. These rocks represent plutonic and volcanic activities that occurred during the Neoproterozoic and possibly also during the Early Cambrian (Fig. 16a). Additionally, the study of xenoliths hosted in granites reveals the occurrence of ortho- and para-derived rocks in the Ventania System basement.

Given the diversity of rock types, their complex structural relationships, and the difficulty of recognizing their original succession, we consider that the term “complex” is more appropriated to refer to the SCI basement rocks. According to this, the Sauce Chico Complex (this work) should replace the Sauce Chico Group (Cuerda et al., 1975). A group comprises two or more formations and its use as a lithostratigraphic unit is practically restricted to sedimentary rocks. The Sauce Chico Complex should also include the Ventania System basement rocks of Early–Middle Cambrian age located outside the SCI (Figs. 3 and 16b): the Cerro Colorado, Agua Blanca, and San Mario granites and the La Ermita and La Mascota rhyolites (Rapela et al., 2003; Tohver et al., 2012). Table 2 summarizes the U–Pb ages of the basement units gathered in the Sauce Chico Complex.

The magmatism registered in the SCI was developed in two main phases, the first one during the Tonian and the second one during the Ediacaran–Early Cambrian (?). These phases involve rocks related to rift and orogenic to post-orogenic environments, respectively. The magmatism registered outside the SCI was developed during the Early–Middle Cambrian and involve rocks related to post-orogenic environment.

Table 2
U–Pb crystallization ages of basement units of the Sauce Chico Complex (Ventania System).

Basement unit	U–Pb method	Age (Ma)	Reference
La Ermita Rhyolite	SHRIMP	505 ± 18	Tohver et al. (2012)
La Ermita Rhyolite	SHRIMP	509.0 ± 5.3	Rapela et al. (2003)
San Mario Granite	SHRIMP	524.3 ± 5.3	Rapela et al. (2003)
Cerro Colorado Granite	SHRIMP	523.8 ± 4.0	Tohver et al. (2012)
Cerro Colorado Granite	SHRIMP	531.1 ± 4.1	Rapela et al. (2003)
Cerro Colorado Granite	SHRIMP	533 ± 12	Tohver et al. (2012)
Cerro Pan de Azúcar Rhyolite	LA-ICP-MS	543.6 ± 4.0	This work
Cerro Pan de Azúcar Granite[a]	SHRIMP	580.8 ± 7.9	Tohver et al. (2012)
Cerro del Corral Ignimbrite	LA-ICP-MS	577.3 ± 3.9	This work
Cerro del Corral Granite	SHRIMP	607.0 ± 5.2	Rapela et al. (2003)
Loma Marcelo Granite	LA-ICP-MS	621.6 ± 2.2	Ballivián Justiniano et al. (2019)
Loma Marcelo Granite	LA-ICP-MS	620.3 ± 2.5	This work
Cerro 21 de Septiembre Granite	LA-ICP-MS	620.8 ± 5.8	This work
Loma Marcelo Orthogneiss	LA-ICP-MS	776.5 ± 4.7	This work
Loma Meyer Granite	LA-ICP-MS	783.8 ± 3.7	This work

[a] The data consigned actually corresponds to the lower intercept age of the Loma Meyer Granite.

The Tonian phase is represented by the intrusion of the 783.8 ± 3.7 Ma calc-alkaline Loma Meyer Granite in metasedimentary rocks of unknown age, followed by the intrusion of the 776.5 ± 4.7 Ma alkaline Loma Marcelo Orthogneiss (Fig. 16a). Although the ages of both units overlap, it is noteworthy that they have geochemical and isotopic differences.

The Ediacaran phase is represented by the Cerro 21 de Septiembre, Loma Marcelo, and Cerro del Corral granites (620.8 ± 5.8 Ma, 620.3 ± 2.5 Ma, and 607.0 ± 5.2 Ma, respectively; Rapela et al., 2003, this work) (Fig. 16a). Although Cerro 21 de Septiembre Granite and Loma Marcelo Granite have similar ages, they differ in some geochemical characteristics (*e.g.*, Eu/Eu*). The Loma Marcelo Granite hosts xenoliths of polymetamorphic sedimentary carbonate rocks, known as Loma Marcelo skarn (Ballivián Justiniano et al., 2017), with maximum and minimum sedimentation ages of 648 ± 21 Ma and 621.6 ± 2.2 Ma, respectively (Ballivián Justiniano et al., 2019). Thus, the age of the Loma Marcelo skarn protolith would be comprised between the Late Cryogenian and the Early Ediacaran (Fig. 16a). The Ediacaran plutonic activity was followed by the extrusion of the 577.3 ± 3.9 Ma alkaline Cerro del Corral Ignimbrite and by the 543.6 ± 4.0 Ma calc-alkaline Cerro Pan de Azúcar Rhyolite (Fig. 16a).

The Early Cambrian magmatic history of the Ventania System is represented by the alkaline Cerro Colorado and Agua Blanca granites (533 ± 12 Ma, 531.1 ± 4.1 Ma, and 523.8 ± 4.0 Ma; Rapela et al., 2003, Tohver et al., 2012) and by the calc-alkaline San Mario Granite (524.3 ± 5.3 Ma; Rapela et al., 2003) (Fig. 16b). Although Rapela et al. (2003) did not find zircons in the Agua Blanca Granite and Tohver et al. (2012) only managed to separate two inherited zircons from this unit, the petrographic and geochemical similarities with the Cerro Colorado Granite suggest a similar genesis and age for both plutonic units. Additionally, in Cerro Pan de Azúcar, rhyolites are cut by an andesite dyke, which could be related to the Early Cambrian calc-alkaline magmatism represented by the San Mario Granite.

The last magmatic event registered in the Ventania System basement, of Middle Cambrian age, is represented by the peralkaline La Ermita and La Mascota rhyolites (509.0 ± 5.3 Ma and 505 ± 18 Ma; Rapela et al., 2003, Tohver et al., 2012) (Fig. 16b). Although Rapela et al. (2003) could not find zircons in the La Mascota Rhyolite, the petrographic and geochemical similarities with the La Ermita Rhyolite suggest a similar genesis and age for both volcanic units.

It should be noted that no geological structures or mineral associations corresponding to Neoproterozoic–Early Palaeozoic metamorphic events have been found in the SCI igneous rocks. This may be due to the superimposed Late Palaeozoic deformation and metamorphism. However, Tohver et al. (2012) obtained a U–Pb zircon age of 580.8 ± 7.9 Ma for the Cerro del Corral Granite, which they interpreted as a lower intercept age. This age is identical to the Ar/Ar muscovite age of 576 ± 5 Ma obtained by Tohver et al. (2012) for what we call here the Loma Meyer Granite. Both ages could be interpreted as corresponding to a metamorphic event.

9.2. Correlation with the Dom Feliciano Belt

The Dom Feliciano Belt (DFB) extends from southern Brazil to the Cuchilla Dionisio Belt in Uruguay (Fig. 2). The most important orogenic activity occurred during the Cryogenian–Cambrian and was related to the closure of the Adamastor Ocean and subsequent collision between the Río de la Plata-Paranapanema cratons and the Congo-Kalahari cratons (*e.g.*, Philipp et al., 2016a; Basei et al., 2018; Hueck et al., 2018). Basement inliers are common and denote intense reworking and magmatism during the Neoproterozoic.

9.2.1. Tonian magmatism

Like the Loma Meyer Granite (*ca.* 784 Ma) and the Loma Marcelo Orthogneiss (*ca.* 777 Ma) of the Sauce Chico Complex, Tonian rocks are also registered in the DFB and the eastern end of the Tandilia System. The Cerro Olivo Complex of the Punta del Este Terrane (Cuchilla Dionisio Belt) is composed of migmatic para- and ortho-derived rocks (*e.g.*, Cerro Bori Orthogneisses; Masquelin et al., 2012). SHRIMP U–Pb zircon dating of these rocks revealed crystallization ages between *ca.* 800 and 760 Ma (Hartmann et al., 2002; Oyhantçabal et al., 2009; Basei et al., 2011; Lenz et al., 2011; Masquelin et al., 2012; Will et al., 2019). Basement inliers of the Pelotas Batholith (Rio Grande do Sul sector of the DFB) consist of medium- to high-grade ortho-derived metamorphic rocks that constitute roof pendants and xenoliths hosted in the granitic suites. SHRIMP U–Pb zircon dating of two of these xenoliths revealed crystallization ages of 781 ± 5 Ma for the Piratini Orthogneiss (Silva et al., 1999) and 777.3 ± 3.6 Ma for the Chácara das Pedras Orthogneiss (Koester et al., 2016). Both in the Cerro Olivo Complex and in the basement inliers of the Pelotas Batholith, metamorphic overgrowths in magmatic zircons yielded ages of *ca.* 650–640 Ma interpreted as the age of a high-grade metamorphic event (Gross et al., 2006; Oyhantçabal et al., 2009; Basei et al., 2011; Lenz et al., 2011; Masquelin et al., 2012; Koester et al., 2016; Martil et al., 2016; Philipp et al., 2016b; Will et al., 2019). Some concordant inherited ages determined in zircon rims of the Loma Marcelo Orthogneiss and in zircon cores and rims of the Loma Marcelo Granite are between *ca.* 641 and 630 Ma. This may further support the correlation of the Sauce Chico Complex with the DFB.

Tonian rocks of the DFB have been interpreted as products of magmatic activity above a subduction zone (Lenz et al., 2011, 2013; Masquelin et al., 2012; Koester et al., 2016) or continental rifting (Oyhantçabal et al., 2010a; Basei et al., 2018; Konopásek et al., 2018;

Will et al., 2019). In the Kaoko, Damara, and Gariep belts of southwestern Africa, the time-lapse *ca.* 840–728 Ma was characterized by alkaline magmatism associated with extension and rifting, related to the break-up of the Rodinia supercontinent (*e.g.*, Hoffman et al., 1996; Frimmel et al., 2001; Jacobs et al., 2008; Konopásek et al., 2008, 2014, 2018). The Loma Marcelo Orthogneiss has alkaline geochemical characteristics that can be related to continental rifting (A_1-type magmatism), also has mantle affinity ($\varepsilon Nd_{777} = +1.65$). On the other hand, the Loma Meyer Granite has calc-alkaline geochemical characteristics and an important crustal component ($\varepsilon Nd_{784} = -7.20$). In a continental rifting context, the calc-alkaline signature of Tonian granitoids like the Loma Meyer Granite can be interpreted as inherited (*e.g.*, Konopásek et al., 2018).

Regarding the Tonian rocks of the Tandilia System, they belong to the Punta Mogotes Formation, cut in a borehole drilled close to Mar del Plata city (eastern end of the Tandilia System) and mainly composed of metasiltstones and metapelites (Rapela et al., 2011). Rapela et al. (2011) obtained detrital zircon age patterns from samples of the Punta Mogotes Formation that exhibit main peaks between *ca.* 840 and 740 Ma. Negative $\varepsilon Hf_{(t)}$ and $\delta^{18}O > 6.5‰$ of these zircons suggest derivation from an old crust as the felsic rocks of the Schist Belt of the DFB. Previously, Cingolani and Bonhomme (1982) obtained K–Ar ages between 615 ± 14 Ma and 515 ± 12 Ma in fine fractions (whole rock) of the Punta Mogotes Formation that was interpreted as a metamorphic overprint. Rapela et al. (2011) proposed a new eastern boundary for the Río de la Plata Craton as a hidden fault that separates the craton from a distinct continental block that they call the "Mar del Plata Terrane" (Fig. 2). The gravimetric anomalies existing to the north of Mar del Plata city, perpendicular to the lengthening of the Tandilia System, were attributed by Kostadinoff (1995) to the continuity of the Brasiliano/Pan-African orogen in Argentina. The contrasting lithology, detrital zircon patterns, and geophysics between the Palaeoproterozoic basement of the Tandilia System and the Punta Mogotes Formation are similar to those observed in Uruguay between the Piedra Alta and Nico Pérez terranes and the DFB (Rapela et al., 2011). Gaucher et al. (2005) and Ramos et al. (2014) considered the Punta Mogotes Formation as part of the "Punta Mogotes Orogen", a large orogen continuous to the DFB to the north and extended southward adjacent to the Río de la Plata Craton.

9.2.2. Cryogenian–Cambrian magmatism

The geochemical data compiled by Bento dos Santos et al. (2015) for the Cryogenian–Early Cambrian evolution of the DFB allowed three stages of magmatic activity to be distinguished (Fig. 17): 1) high-K calc-alkaline syn-orogenic magmatism with metaluminous to peraluminous affinity, 2) followed by a post-orogenic calc-alkaline (I-type) and alkaline (A-type) magmatism, and, finally, 3) peralkaline magmatism. The same evolutionary sequence can be observed in the Ediacaran–Middle Cambrian rocks of the Sauce Chico Complex (Rapela et al., 2003; this work).

The Cerro 21 de Septiembre, Loma Marcelo, and Cerro del Corral granites (*ca.* 621–607 Ma) are coeval with similar granite emplacement in southern Brazil and Uruguay associated with the closure of the Adamastor Ocean (see Section 9.4). A compilation of high-resolution U–Pb geochronology and geochemistry made by Bento dos Santos et al. (2015) limits the period of syn-orogenic magmatic activity of the DFB to the interval *ca.* 623–593 Ma. The Cerro del Corral Granite was considered by Rapela et al. (2003) as the southernmost exposure of the DFB. Like the Cryogenian granites of the SCI (Rapela et al., 2003; this work), the granitic suites of the Florianópolis, Pelotas, and Aiguá batholiths of the DFB, known as the Granite Belt, are high-K calc-alkaline with metaluminous to peraluminous affinity and were originated by anatexis of older crustal rocks (Koester et al., 2001a; Philipp et al., 2003, 2008, 2013, 2016a).

The last stages of magmatism and sedimentation of the DFB developed between *ca.* 590 and 500 Ma, mostly between *ca.* 590 and 550 Ma

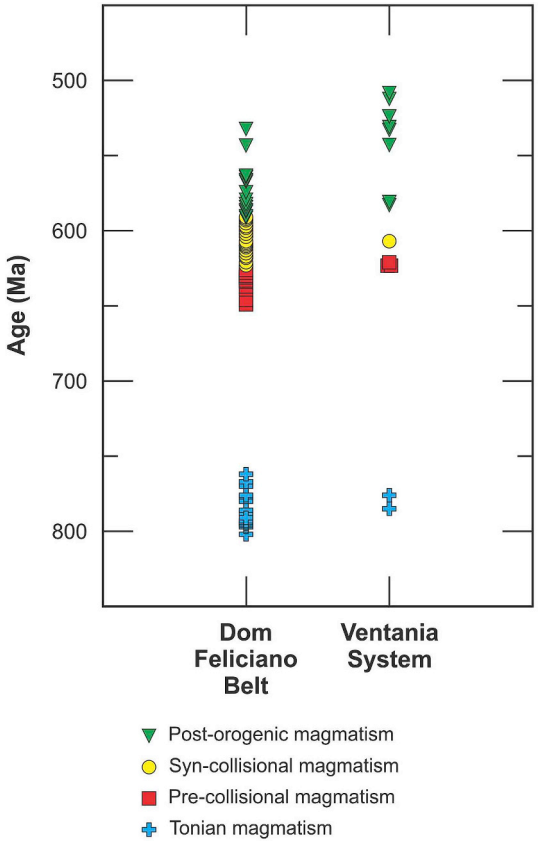

Fig. 17. Compilation of high-resolution U–Pb geochronology that shows consistency between the magmatic evolution of the Dom Feliciano Belt and that of the Sauce Chico Complex. The red squares and yellow circles represent the syn-orogenic magmatism of high-K calc-alkaline and metaluminous to peraluminous affinity. The green triangles represent the post-orogenic magmatism of calc-alkaline (I-type) and alkaline to peralkaline (A-type) affinity. Based on the U–Pb zircon dataset compiled by Bento dos Santos et al. (2015) for the Dom Feliciano Belt and the available U–Pb zircon ages for the Sauce Chico Complex (Rapela et al., 2003; Tohver et al., 2012; Ballivián Justiniano et al., 2019; this work). (For interpretation of the references to colour in this figure legend, the reader is referred to the Web version of this article.)

(*e.g.*, Philipp et al., 2016a). In southern Brazil, late- to post-orogenic magmatism of the Pelotas Batholith is represented by the alkaline and peralkaline Piquiri and Encruzilhada do Sul suites (612 ± 3 Ma to 595 ± 4 Ma; Babinski et al., 1997, Philipp et al., 2002) and by the high-K calc-alkaline to alkaline Dom Feliciano Suite (*e.g.*, 600 ± 3 Ma; Koester et al., 2001b). In Uruguay, U–Pb zircon ages of individual intrusions forming the Aiguá Batholith are between *ca.* 616 and 564 Ma (Basei et al., 2000; Oyhantçabal et al., 2007; Gaucher et al., 2014; Lara et al., 2016). Numerous granite bodies emplaced west of the Aiguá Batholith, in the Nico Pérez Terrane, have ages between 634 ± 7 Ma (Sierra de los Caracoles Granite, LA-ICP-MS U–Pb zircon age; Lara et al., 2017) and 583 ± 7 Ma (Mangacha Granite, SIMS U–Pb zircon age; Gaucher et al., 2008). East of the Aiguá Batholith, in the Punta del Este Terrane, granitic bodies have ages between 590 ± 25 Ma (José Ignacio Granite, Rb–Sr isochron age; Umpierre and Halpern, 1971) and 543 ± 7 Ma (Santa Teresa Granitic Complex, LA-ICP-MS U–Pb zircon age; Basei et al., 2013). Whole rock geochemistry of the Uruguayan plutonic rocks indicate signatures that range from highly fractionated high-K calc-alkaline (*e.g.*, Aiguá Pluton; Gómez Rifas, 1995) to transitional features between calc-alkaline and alkaline (*e.g.*, Maldonado Granite; Oyhantçabal et al., 2007) with metaluminous to peraluminous affinity (see also Lara et al., 2017).

Acid volcanic rocks of similar age and composition to that of the Cerro del Corral Ignimbrite (*ca.* 577 Ma) and the Cerro Pan de Azúcar

Rhyolite (*ca.* 544 Ma) can be found in southern Brazil and eastern Uruguay. Rhyolitic rocks of southern Brazil have U–Pb ages of 581.9 ± 1.9 Ma (Ana Dias Rhyolite; Oliveira et al., 2015), 579.1 ± 5.6 Ma (Acampamento Velho Formation; Sommer et al., 2017), and 549.0 ± 5.0 Ma (Ramada Plateau; Sommer et al., 2005). In Uruguay, volcanic and volcaniclastic rocks have U–Pb ages of 573 ± 11 Ma (volcaniclastic rocks of the Las Ventanas Formation; Oyhantçabal et al., 2009), 571 ± 8 Ma (dacitic ignimbrite of the Sierra de Aguirre Formation; Hartmann et al., 2002), and 567.4 ± 7.9 Ma (Sierra de Rios Rhyolite; Will et al., 2019). For the Acampamento Velho Formation, Sommer et al. (2017) reported Nd and Pb isotopic data that indicate variable amounts of melting from a lower crust of Palaeoproterozoic age in a post-collisional to intraplate environment. For the Sierra de Rios Rhyolite, Will et al. (2019) reported Nd and Hf isotopic data that indicate the recycling of Mesoproterozoic crust or mixing of juvenile material with pre-existing continental crust.

The geochemical data obtained by Rapela et al. (2003) and Gregori et al. (2005) for the Cambrian basement of the Ventania System has similarities with the geochemical data compiled by Bento dos Santos et al. (2015) for the late- to post-orogenic magmatism of the DFB. This magmatism is related to shear zones associated with the granitogenesis of the Granite Belt (Hueck et al., 2019 and references therein) and with transtensional to extensional environments in the foreland basins (*e.g.*, Philipp et al., 2016a). Post-orogenic calc-alkaline and alkaline magmatism could be related to slab break-off, asthenospheric upwelling, and orogenic collapse of the collisional orogen (*e.g.*, Bento dos Santos et al., 2015).

Rapela et al. (2003) related the Neoproterozoic granites (*ca.* 607 Ma) to the closure of the Adamastor Ocean and the Cambrian magmatism to a continental rift that began with the shallow emplacement of A_2- and I-type granites during the Early Cambrian (*ca.* 531–524 Ma) and culminated with extrusion of the A_1-type rhyolites during the Middle Cambrian (*ca.* 509 Ma). Chemale et al. (2011) pointed out the existence of lithogeochemical and isotopic similarities between the A- and I-type igneous rocks of the Ventania System and those of the Saldania Belt (*ca.* 540–500 Ma). However, it is worth highlighting the older age of the S-type granites of the Ventania System (*ca.* 607 Ma; Rapela et al., 2003) than that of granites of the Saldania Belt (*ca.* 550–527 Ma; Chemale et al., 2011).

9.3. Source of the Sauce Chico Complex basement rocks

The inherited ages of the Sauce Chico Complex basement rocks analysed in this work extend from the Orosirian to the Tonian. Four $^{207}Pb/^{235}U$ concordant ages correspond to the Orosirian (*ca.* 1996–1867 Ma), two to the Statherian (*ca.* 1777 and 1643 Ma), five to the Mesoproterozoic (*ca.* 1439–1087 Ma), and six to the Tonian (*ca.* 854–792 Ma). Rapela et al. (2003) registered a $^{207}Pb/^{206}Pb$ concordant inherited age of *ca.* 965 Ma in the Cerro del Corral Granite (*ca.* 607 Ma). On the other hand, Tohver et al. (2012) registered $^{207}Pb/^{206}Pb$ inherited ages of *ca.* 2169 and 2196 Ma in the Agua Blanca Granite (upper intercept at 2182 ± 18 Ma). Some of the above mentioned Palaeoproterozoic inherited ages are close to the time interval corresponding to the magmatic climax (*ca.* 2250–2120 Ma) registered in the Tandilia System basement (Cingolani, 2011). However, it should be noted that most of the remaining inherited ages are within the time interval corresponding to the magmatic activity registered in the Namaqua Metamorphic Complex (Eglington, 2006; Oriolo and Becker, 2018), which is located in the Namaqua Belt and exposed in the Gariep Belt on the west coasts of Namibia and South Africa (Fig. 2).

As in the Sauce Chico Complex, Tonian rocks of the DFB have inherited ages between *ca.* 2.1 and 0.8 Ga, with a significant concentration of ages between *ca.* 1.3 and 0.9 Ga (Silva et al., 1999; Hartmann et al., 2002; Oyhantçabal et al., 2009; Basei et al., 2011; Lenz et al., 2011; Masquelin et al., 2012; Koester et al., 2016). Preciozzi et al. (1999) proposed the correlation between the Punta del Este Terrane and the Namaqua Metamorphic Complex. Subsequent studies carried out on rocks from both sides of the South Atlantic Ocean would confirm this correlation (Basei et al., 2000, 2005, 2011; Frimmel et al., 2011, 2013; Masquelin et al., 2012). However, this is still a matter of debate, since several works also point out a correlation of the Punta del Este Terrane with the Coastal Terrane of the Kaoko Belt (Fig. 2), which is the African counterpart of the Granite Belt (Goscombe et al., 2005; Gross et al., 2006; Goscombe and Gray, 2007; Oyhantçabal et al., 2009; Lenz et al., 2011; Konopásek et al., 2014, 2018).

9.4. Tectonic evolution of the Dom Feliciano Belt and the Sauce Chico Complex

The tectonic model described below is based on that synthesized by Basei et al. (2018) in which the Sauce Chico Complex was incorporated. Tonian rocks of the DFB and the Sauce Chico Complex represent the break-up of the Rodinia supercontinent and related continental rifting. It should be noted that the Punta Mogotes Formation of the Tandilia System contains *ca.* 840–740 Ma detrital zircons that Rapela et al. (2011) assigned to the Tonian rifting event. These authors proposed a source close to the Angola Block, from which the Mar del Plata Terrane rifted away during the opening of the Adamastor Ocean. Alternatively, these rocks could be correlated with the Coastal Terrane of the Kaoko Belt, which is adjacent to the Angola Craton.

After ocean floor spreading and development of passive margin deposits on both sides of the Adamastor Ocean, a convergence regime was installed (*ca.* 650–630 Ma). Subduction of the Adamastor Ocean would have occurred towards the east (present coordinates), generating a magmatic arc along the western margin of the Kalahari Craton. The collision of the cratonic nuclei located on both sides of the Adamastor Ocean would have juxtaposed the magmatic arc to the passive margin deposits developed along the eastern margins of the Río de la Plata Craton. The final closure of the Adamastor Ocean would have occurred during the Ediacaran (~ 600 Ma). The Major Gercino-Dorsal do Canguçu-Sierra Ballena Shear Zone (Fig. 2) would represent the suture zone (*e.g.*, Passarelli et al., 2011a, 2011b; Oriolo et al., 2018). These shear zones defined by transcurrent mylonitic belts, particularly evident in the Pelotas Batholith, were active during the development of the Granite Belt and controlled the emplacement of granitic suites (Fernandes et al., 1992; Koester et al., 2001b; Philipp et al., 2003; Oyhantçabal et al., 2009). A slightly different model considers the suture zone along the Sarandí del Yí Shear Zone (*e.g.*, Oriolo et al., 2016). A post-collisional magmatism would have developed due to orogenic collapse (< 580 Ma).

Fig. 2 shows that the Sauce Chico Complex is displaced towards the west (present coordinates) in relation to the Brasiliano/Pan-African magmatic axis. The contact between the Río de la Plata Craton to the west and the Kalahari Craton to the east would be marked by what we call here the Punta Mogotes Fault. This fault is the southern continuity of the Sarandí del Yí Shear Zone. The Major Gercino-Dorsal do Canguçu-Sierra Ballena Shear Zone system coalesce towards the south with the former, which is the margin of the Río de la Plata Craton. The Sierra de la Ventana Fault (Rapela et al., 2011) could have been responsible for the dextral displacement of part of the Brasiliano/Pan-African magmatic axis to its current position in the southwestern sector of the Buenos Aires Province (Fig. 18). Rapela et al. (2011) have already suggested that the Ventania System basement could have been dextrally transported from the Saldania Belt.

The opening of the South Atlantic Ocean during the Cretaceous, mostly along the back-arc region of the Brasiliano/Pan-African orogen, left in South America a large part of the magmatic arc (Granite Belt), as well as the Punta del Este Terrane, the Mar del Plata Terrane/Punta Mogotes Orogen, and the Sauce Chico Complex. They constitute African remnants reworked before and after the collision that contributed to the construction of the current South American Platform.

One aspect worth mentioning is the southern boundary of the Río de

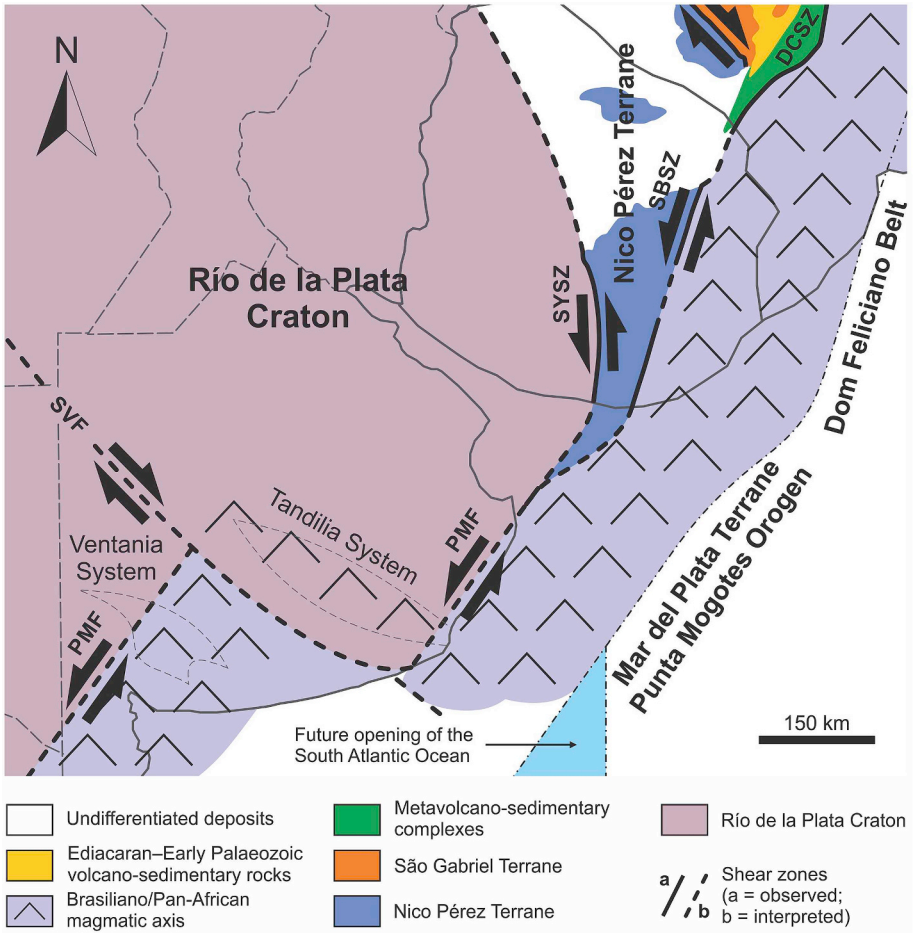

Fig. 18. Correlation of the Ventania System basement with the Dom Feliciano Belt and its southern continuity in the Mar del Plata Terrane/Punta Mogotes Orogen (Gaucher et al., 2005; Rapela et al., 2011; Ramos et al., 2014). The Ventania System basement is dextrally transported to its current position through the Sierra de la Ventana Fault. This fault would have formed after the sinestral displacement of the Punta Mogotes Fault and before the beginning of the sedimentation of the Curamalal Group (Middle/Late Cambrian). **Abbreviations:** DCSZ = Dorsal do Canguçu Shear Zone, SBSZ = Sierra Ballena Shear Zone, SYSZ = Sarandí del Yí Shear Zone, PMF = Punta Mogotes Fault, SVF = Sierra de la Ventana Fault.

la Plata Craton. Several authors proposed different limits for this craton (*e.g.*, Rapela et al., 2007, 2011; Oyhantçabal et al., 2010b, 2018b). Based on their U–Pb zircon data, Rapela et al. (2003) and Tohver et al. (2012) provided some hints regarding the relation between the Ventania System basement and the Río de la Plata Craton. Our new data clearly shows the presence of an orogeny in the area. This implies that the craton boundary may be located further north and the Ventania System basement can be ruled out as the southern exposure of the craton (Fig. 2).

10. Conclusions

Our new geological, geochemical, and geochronological data on basement rocks cropping out at the Sauce Chico Inlier allow a better understanding of the tectonic evolution of the Ventania System basement as a whole, here named Sauce Chico Complex. These results include the first evidence of Tonian magmatism in the Ventania System basement and confirm those obtained previously by other authors regarding Ediacaran–Cambrian magmatism (*e.g.*, Rapela et al., 2003; Gaucher et al., 2005; Tohver et al., 2012; Ramos et al., 2014). Based on the available data, the following evolution of the Sauce Chico Complex is proposed:

1) Break-up of the Rodinia supercontinent and continental rifting, which is represented by the Loma Meyer Granite (783.8 ± 3.7 Ma; $\varepsilon Nd_{784} = -7.20$; $T_{DM} = 1.73$ Ga) and the Loma Marcelo Orthogneiss (776.5 ± 4.7 Ma; $\varepsilon Nd_{777} = +1.65$; $T_{DM} = 1.14$ Ga). The presence of metapelitic xenoliths in the Loma Meyer Granite records the pre-784 Ma sedimentation. These Tonian rocks of the Sauce Chico Complex are correlated with rocks of similar age of the Dom Feliciano Belt that crop out in the Cerro Olivo Complex of the Punta del Este Terrane and as basement inliers in the Pelotas Batholith.
2) After ocean floor spreading and once a convergence regime was installed (*ca.* 650–630 Ma), subduction of oceanic crust occurred, generating a magmatic arc along the western margin of the Kalahari Craton. This was followed by the closure of the Adamastor Ocean and the collision between the Río de la Plata and Kalahari cratons. The syn-orogenic period with calc-alkaline magmatism is represented by the Cerro 21 de Septiembre, Loma Marcelo, and Cerro del Corral granites (620.8 ± 5.8 Ma, 620.3 ± 2.5 Ma, and 607.0 ± 5.2 Ma, respectively; $\varepsilon Nd_{(t)} = -9.94/-9.18$; $T_{DM} = 1.80$–1.66 Ga).
3) Post-orogenic period with alkaline and calc-alkaline magmatism represented by the Cerro del Corral Ignimbrite (577.3 ± 3.9 Ma; $\varepsilon Nd_{577} = -6.29$; $T_{DM} = 1.73$ Ga) and the Cerro Pan de Azúcar Rhyolite (543.6 ± 4.0 Ma; $\varepsilon Nd_{544} = -3.38$; $T_{DM} = 1.32$ Ga), respectively. Outside the Sauce Chico Inlier, the alkaline Cerro Colorado and Agua Blanca granites (*ca.* 533–524 Ma), the calc-alkaline San Mario Granite (*ca.* 524 Ma), and the peralkaline La Ermita and La Mascota rhyolites (*ca.* 509–505 Ma) constitute the Early–Middle Cambrian post-orogenic magmatism of the Sauce Chico Complex. As in the Dom Feliciano Belt, the post-orogenic magmatism of the Sauce Chico Complex could be related to slab break-off, asthenospheric upwelling, and orogenic collapse of the collisional orogen.
4) Calymmian to Tonian inherited ages registered in the Sauce Chico Complex could indicate a lineage with the Gariep Belt and its Namaqua metamorphic basement. A similar origin is interpreted for the Cerro Olivo Complex of the Punta del Este Terrane (southern

Dom Feliciano Belt).

5) Nd model ages (T_{DM}) of the SCI basement rocks may result from the mixing of older crust (Mesoproterozoic, Palaeoproterozoic, or even older) with juvenile material of Neoproterozoic age. Even reworking of Tonian rocks might contribute as well. The geochronological and isotopic results would suggest different contributions of juvenile and reworked older crust.
6) The boundary of the Río de la Plata Craton may be located north of the Ventania System and the Sauce Chico Complex can be ruled out as the southern exposure of the craton.

Acknowledgements

We would like to acknowledge R.E. de Barrio, M. Naipauer, N.J. Uriz, M.A. Comerio, M.L. Gómez Samus, G.A. Greco, and J.M. Susena for their help during the fieldworks. We also acknowledge the Ducos family for allowing us to work in their farms and the CPGeo staff and the Quirino family for the hospitality given to the first author during his stay in São Paulo, Brazil. This study was supported by a postdoctoral research fellowship awarded to the first author by the Consejo Nacional de Investigaciones Científicas y Técnicas (CONICET) of Argentina. Research grants awarded by the Comisión de Investigaciones Científicas de la Provincia de Buenos Aires, the Universidad Nacional de La Plata (N 617, N 716, N 778, N 860, Viajes y Estadías 2017), and own funds of the first author also supported this study. We warmly acknowledge the comments and suggestions made by Carlos W. Rapela and Jiri Konopásek, which improved the original manuscript considerably. We also acknowledge the reviews of Sebastián Oriolo and two anonymous reviewers.

Appendix A. Supplementary data

Supplementary data to this article can be found online at https://doi.org/10.1016/j.jsames.2019.102391.

References

Andreis, R.R., Iñíguez, A.M., Lluch, J.L., Rodríguez, S., 1989. Cuenca paleozoica de Ventania, sierras Australes, provincia de Buenos Aires. In: Chebli, G.A., Spalletti, L.A. (Eds.), Cuencas Sedimentarias Argentinas. Instituto Superior de Correlación Geológica, Serie Correlación Geológica 6. San Miguel de Tucumán, Argentina, pp. 265–298.

Babinski, M., Chemale Jr., F., Van Schmus, W.R., Hartmann, L.A., Silva, L.C., 1997. U-Pb and Sm-Nd geochronology of the Neoproterozoic granitic-Gneissic Dom Feliciano belt, southern Brazil. J. South Am. Earth Sci. 10, 263–274.

Ballivián Justiniano, C.A., Lanfranchini, M.E., Recio Hernández, C., de Barrio, R.E., Sato, A.M., Basei, M.A.S., Pimentel, M.M., Etcheverry, R.O., Tassinari, C.C.G., 2017. Geology and petrogenetic considerations of the loma Marcelo skarn, Neoproterozoic basement of the Ventania system, Argentina. Precambrian Res. 302, 358–380.

Ballivián Justiniano, C.A., Lajoinie, M.F., Recio, C., Sato, A.M., Basei, M.A.S., Proenza Fernández, J.A., Aiglsperger, T.H., de Barrio, R.E., Curci, M.V., Lanfranchini, M.E., 2019. Metamorphic evolution of the Loma Marcelo skarn within the geotectonic context of the crystalline basement of the Ventania System (Argentina). J. South Am. Earth Sci. 92, 56–76.

Barker, F., 1979. Trondhjemites: definition, environment and hypothesis of origin. In: Barker, F. (Ed.), Trondhjemites, Dacites and Related Rocks. Elsevier, Amsterdam, pp. 1–12.

Basei, M.A.S., Frimmel, H.E., Nutman, A.P., Preciozzi, F., 2008. West Gondwana amalgamation based on detrital zircon ages from Neoproterozoic Ribeira and Dom Feliciano belts of South America and comparison with coeval sequences from SW Africa. In: In: Pankhurst, R.J., Trouw, R.A.J., Brito Neves, B.B., de Wit, M.J. (Eds.), West Gondwana: Pre-cenozoic Correlations across the South Atlantic Region, vol. 294. Geological Society Special Publications, London, pp. 239–256.

Basei, M.A.S., Sánchez-Bettucci, L., Peel, E., Muzio, R., 2013. Geocronología U-Pb LA-ICP-MS en circones del Complejo Granítico Santa Teresa, Terreno Punta del Este. In: 7° Congreso Uruguayo de Geología. Actas, Montevideo, pp. 30–31.

Basei, M.A.S., Frimmel, H.E., Nutman, A.P., Preciozzi, F., Jacob, J., 2005. A connection between the Neoproterozoic Dom Feliciano (Brazil/Uruguay) and Gariep (Namibia/South Africa) orogenic belts – evidence from a reconnaissance provenance study. Precambrian Res. 139, 195–221.

Basei, M.A.S., Peel, E., Sánchez Bettucci, L., Preciozzi, F., Nutman, A.P., 2011. The basement of the Punta del Este Terrane (Uruguay): an African Mesoproterozoic fragment at the eastern border of the South American Río de La Plata craton. Int. J. Earth Sci. 100, 289–304.

Basei, M.A.S., Frimmel, H.E., Campos Neto, M. da C., de Araujo, C.E.G., de Castro, N.A., Passarelli, C.R., 2018. The tectonic history of the southern Adamastor Ocean based on a correlation of the Kaoko and Dom Feliciano belts. In: Siegesmund, S., Basei, M.A.S., Oyhantçabal, P., Oriolo, S. (Eds.), Geology of Southwest Gondwana. Regional Geology Reviews, Cham, pp. 63–85.

Basei, M.A.S., Siga Jr., O., Masquelin, H., Harara, O.M., Reis Neto, J.M., Preciozzi, F., 2000. The Dom Feliciano belt of Brazil and Uruguay and its foreland domain the Rio de la Plata craton: framework, tectonic evolution and correlation with similar provinces of southwestern Africa. In: Cordani, U.G., Milani, E.J., Thomaz Filho, A., Campos, D.A. (Eds.), Tectonic evolution of South America. 31° International Geological Congress, Rio de Janeiro, pp. 311–334.

Bento dos Santos, T.M., Tassinari, C.C.G., Fonseca, P.E., 2015. Diachronic collision, slab break-off and long-term high thermal flux in the Brasiliano–Pan-African orogeny: implications for the geodynamic evolution of the Mantiqueira Province. Precambrian Res. 260, 1–22.

Best, M.G., 2003. Igneous and Metamorphic Petrology. Blackwell Publishing, Oxford.

Borrello, A.V., Venier, J., 1967. Nuevos caracteres geológicos del granito de Aguas Blancas, Dufaur, provincia de Buenos Aires. In: Anales de la Comisión de Investigaciones Científicas de la Provincia de Buenos Aires, vol. 5. pp. 3–8.

Buggisch, W., 1987. Stratigraphy and very low-grade metamorphism of the Sierras Australes de la Provincia de Buenos Aires (Argentina) and implications in Gondwana correlation. Zentralbatt für Geologie Paläontologie, Teil I (7/8), 819–837.

Cazeneuve, H., 1967. Edades isotópicas del basamento de la provincia de Buenos Aires. Ameghiniana 5, 3–10.

Chemale Jr., F., Scheepers, R., Gresse, P.G., Van Schmus, W.R., 2011. Geochronology and sources of late Neoproterozoic to Cambrian granites of the Saldania belt. Int. J. Earth Sci. 100, 431–444.

Cingolani, C.A., 2011. The Tandilia System of Argentina as a southern extension of the Río de la Plata craton: an overview. Int. J. Earth Sci. 100, 221–242.

Cingolani, C.A., Bonhomme, M.G., 1982. Geochronology of La Tinta upper Proterozoic sedimentary rocks, Argentina. Precambrian Res. 18, 119–132.

Cingolani, C.A., Varela, R., 1973. Examen geocronológico por el método Rubidio-Estroncio de las rocas ígneas de las Sierras Australes Bonaerenses. In: 5° Congreso Geológico Argentino, vol. 1. Actas, Buenos Aires, pp. 349–371.

Cobbold, P.R., Massabie, A.C., Rossello, E.A., 1986. Hercynian wrenching and thrusting in the sierras Australes Foldbelt, Argentina. Hercynica 2, 135–148.

Cordani, U.G., Pimentel, M.M., Ganade de Araújo, C.E., Fuck, R.A., 2013. The significance of the Transbrasiliano-Kandi tectonic corridor for the amalgamation of West Gondwana. Braz. J. Geol. 43, 583–597.

Cucchi, R.J., 1966. Petrofábrica del conglomerado de la Formación La Lola, Sierras Australes de la provincia de Buenos Aires. Rev. Asoc. Geol. Argent. 21, 71–106.

Cuerda, A.J., Cingolani, C.A., Barranquero, H.R., 1975. Estratigrafía del basamento precámbrico en la comarca de los cerros Pan de Azúcar-del Corral, Sierras Australes (Provincia de Buenos Aires). In: 2° Congreso Iberoamericano de Geología Económica, vol. 1. Actas, Buenos Aires, pp. 57–63.

DePaolo, D.J., 1981. Neodymium isotopes in the Colorado Front Range and crust–mantle evolution in the Proterozoic. Nature 291, 193–196.

Eby, G.N., 1990. The A-type granitoids: a review of their occurrence and chemical characteristics and speculations on their petrogenesis. Lithos 26, 115–134.

Eby, G.N., 1992. Chemical subdivision of the A-type granitoids: petrogenetic and tectonic implications. Geology 20, 641–644.

Eglington, B.M., 2006. Evolution of the Namaqua-Natal Belt, southern Africa – a geochronological and isotope geochemical review. J. Afr. Earth Sci. 46, 93–111.

Fernandes, L.A., Tommasi, A., Porcher, C.C., 1992. Deformation patterns in the southern Brazilian branch of the Dom Feliciano Belt, a reappraisal. J. South Am. Earth Sci. 5, 77–96.

Frimmel, H.E., Basei, M.S., Gaucher, C., 2011. Neoproterozoic geodynamic evolution of SW-Gondwana: a southern African perspective. Int. J. Earth Sci. 100, 323–354.

Frimmel, H.E., Zartman, R.E., Späth, A., 2001. The Richstersveld Igneous Complex, South Africa: U–Pb zircon and geochemical evidence for the beginning of the Neoproterozoic continental break-up. J. Geol. 109, 493–508.

Frimmel, H.E., Basei, M.A.S., Correa, V.X., Mbangula, N., 2013. A new lithostratigraphic subdivision and geodynamic model for the Pan-African western Saldania Belt, South Africa. Precambrian Res. 231, 218–235.

Gaucher, C., Frei, R., Frei, D., Blanco, G., 2014. Edad, proveniencia y paleogeografía de la Formación San Carlos. In: Bossi, J., Gaucher, C. (Eds.), Geología del Uruguay - Tomo 1: Predevónico. UdelaR, Montevideo.

Gaucher, C., Poiré, D.G., Gómez Peral, L., Chiglino, L., 2005. Litoestratigrafía, bioestratigrafía y correlaciones de las sucesiones sedimentarias del Neoproterozoico-Cámbrico del Cratón del Río de la Plata (Uruguay y Argentina). Lat. Am. J. Sedimentol. Basin Anal. 12, 145–160.

Gaucher, C., Finney, S.C., Poiré, D.G., Valencia, V.A., Grove, M., Blanco, G., Pamoukaghlián, K., Gómez Peral, L., 2008. Detrital zircon age of Neoproterozoic sedimentary successions of Uruguay and Argentina: insights into the geological evolution of the Río de la Plata Craton. Precambrian Res. 167, 150–170.

Goldstein, S.L., O'Nions, R.K., Hamilton, P.J., 1984. A Sm-Nd study of atmospheric dusts and particulates from major river systems. Earth Planet. Sci. Lett. 70, 221–236.

Gómez Rifas, C., 1995. A Zona de Cisalhamento Sinistral "Sierra Ballena" no Uruguai. Ph.D. thesis. Universidade de São Paulo.

González, P.D., Páez, G.N., Cervera, F.M., Iribarne, M., 2004. Texturas relícticas en las metaignimbritas neoproterozoicas del basamento del cerro del Corral, Sierras Australes de Buenos Aires. Rev. Asoc. Geol. Argent. 59, 103–112.

Goscombe, B.D., Gray, D., 2007. The coastal terrane of the Kaoko belt, Namibia: outboard arc terrane and tectonic significance. Precambrian Res. 155, 139–158.

Goscombe, B., Gray, D., Armstrong, R., Foster, D.A., Vogl, J., 2005. Event geochronology of the pan-African Kaoko belt, Namibia. Precambrian Res. 140 103.e1–103.e41.

Grecco, L.E., Delpino, S.H., Gregori, D.A., Dimieri, L.V., 2000. Evaluación de la movilidad de elementos mayoritarios y traza durante la milonitización de rocas del basamento de las Sierras Australes de Buenos Aires. Rev. Asoc. Geol. Argent. 55, 352–362.
Gregori, D.A., López, V.L., Grecco, L.E., 2005. A late Proterozoic–early Paleozoic magmatic Cycle in Sierra de la Ventana, Argentina. J. South Am. Earth Sci. 19, 155–171.
Gross, A.O.M.S., Porcher, C.C., Fernandes, L.A.D., Koester, E., 2006. Neoproterozoic low-pressure/high-temperature colisional metamorphic evolution in the Varzea do Capivarita Metamorphic Suite, SE Brazil: Thermobarometric and Sm/Nd evidence. Precambrian Res. 147, 41–64.
Halpern, M., Umpierre, M., Linares, E., 1970. Radiometric ages of crystalline rocks from southern South America as related to Gondwana and Andean geologic provinces. In: Conferencia Problemas sobre la Tierra Sólida, vol. 2. Actas, Buenos Aires, pp. 345–356.
Hamilton, P.J., O'Nions, P.K., Bridgwater, D., Nutman, A., 1983. Sm-Nd studies of Archaean metasediments and metavolcanics from West Greenland and their implications for the Earth's early history. Earth Planet. Sci. Lett. 62, 263–272.
Harrington, H.J., 1947. Explicación de las Hojas Geológicas 33m y 34m, Sierras de Curamalal y de la Ventana, Provincia de Buenos Aires, vol. 61 Dirección de Minas y Geología, Boletín, Buenos Aires.
Harrington, H.J., 1972. Sierras Australes de Buenos Aires. In: Leanza, A.F. (Ed.), Geología Regional Argentina. Academia Nacional de Ciencias, Córdoba, Argentina, pp. 395–405.
Hartmann, L.A., Santos, J.O.S., Bossi, J., Campal, N., Schipilov, A., McNaughton, N.J., 2002. Zircon and titanite U–Pb SHRIMP geochronology of Neoproterozoic felsic magmatism on the eastern border of the Rio de la Plata Craton, Uruguay. J. South Am. Earth Sci. 15, 229–236.
Heilbron, M., Valeriano, C.M., Tassinari, C.C.G., Almeida, J.C.H., Tupinamba, M., Siga, O., Trouw, R.A.J., 2008. Correlation of Neoproterozoic terranes between the Ribeira Belt, SE Brazil and its African counterpart: comparative tectonic evolution and open questions. In: In: Pankhurst, R.J., Trouw, R.A.J., Brito Neves, B.B., de Wit, M.J. (Eds.), West Gondwana: Pre-cenozoic Correlations across the South Atlantic Region, vol. 294. Geological Society Special Publications, London, pp. 211–237.
Hoffman, P.F., Hawkins, D.P., Isachsen, C.E., Bowring, S.A., 1996. Precise U–Pb zircon ages for early Damaran magmatism in the Summas mountains and welwitschia inlier, northern Damara belt, Namibia. Commun. Geol. Surv. Namib. 11, 47–52.
Hueck, M., Oyhantçabal, P., Philipp, R.P., Basei, M.A.S., Siegesmund, S., 2018. The Dom Feliciano belt in southern Brazil and Uruguay. In: Siegesmund, S., Basei, M.A.S., Oyhantçabal, P., Oriolo, S. (Eds.), Geology of Southwest Gondwana. Regional Geology Reviews, Cham, pp. 267–302.
Hueck, M., Basei, M.A.S., Wemmer, K., Oriolo, S., Heidelbach, F., Siegesmund, S., 2019. Evolution of the major Gercino shear zone in the Dom Feliciano belt, south Brazil, and implications for the assembly of southwestern Gondwana. Int. J. Earth Sci. 108, 403–425.
Irvine, T.N., Baragar, W.R.A., 1971. A Guide to the chemical classification of the common volcanic rocks. Can. J. Earth Sci. 8, 523–548.
Jackson, S.E., Pearson, N.J., Griffin, W.L., Belousova, E.A., 2004. The application of laser ablation-inductively coupled plasma-mass spectrometry to in situ U–Pb zircon geochronology. Chem. Geol. 211, 47–69.
Jacobs, J., Pisarevsky, S., Thomas, R.J., Becker, T., 2008. The Kalahari craton during the assembly and dispersal of Rodinia. Precambrian Res. 160, 142–158.
Japas, M.S., 1987. Caracterización geométrico-estructural del Grupo Pillahuincó. II. Formación Sauce Grande. Perfil del Cordón Mambacher y Sierra de las Tunas Occidental, Sierras Australes de Buenos Aires. Anales de la Academia Nacional de Ciencias Exactas, Físicas y Naturales (Buenos Aires) 39, 125–144.
Kilmurray, J.O., 1968a. Petrología de las rocas ígneas de las Sierras Australes de la Provincia de Buenos Aires. Rev. Mus. La Plata 6, 155–188.
Kilmurray, J.O., 1968b. Petrología de las rocas cataclásticas y el skarn del anticlinal del Cerro Pan de Azúcar (Partido de Saavedra, Provincia de Buenos Aires). In: 3° Jornadas Geológicas Argentinas, Buenos Aires, vol. 3. Actas, pp. 217–238.
Kilmurray, J.O., 1975. Las Sierras Australes de la Provincia de Buenos Aires. Las fases de deformación y nueva interpretación estratigráfica. Rev. Asoc. Geol. Argent. 30, 331–348.
Koester, E., Roisenberg, A., Fernandes, L.A.D., Soliani Jr., E., Nardi, L.V.S., Kraemer, G., 2001a. Petrologia dos granitóides sintectônicos à Zona de Cisalhamento Transcorrente Dorsal de Canguçu, Encruzilhada do Sul, RS. Rev. Bras. Geociencias 31, 131–140.
Koester, E., Porcher, C.C., Pimentel, M.M., Fernandes, L.A.D., Vignol-Lelarge, M.L., Oliveira, L.D., Ramos, R.C., 2016. Further evidence of 777 Ma subduction-related continental arc magmatism in Eastern Dom Feliciano Belt, southern Brazil: the Chácara das Pedras Orthogneiss. J. South Am. Earth Sci. 68, 155–166.
Koester, E., Soliani Jr., E., Leite, J.A.D., Hartmann, L.A., Fernandes, L.A.D., Santos, J.O.S., Oliveira, L.D., 2001b. SHRIMP U-Pb age for the emplacement of Santana granite and reactivation of the Porto Alegre Suture, southern Brazil. J. South Am. Earth Sci. 14, 91–99.
Kollenz, S., Glasmacher, U.A., Rossello, E.A., Stockli, D.F., Schad, S., Pereyra, R.E., 2017. Thermochronological constraints on the Cambrian to recent geological evolution of the Argentina passive continental margin. Tectonophysics 716, 182–203.
Konopásek, J., Košler, J., Sláma, J., Janoušek, V., 2014. Timing and sources of pre-collisional Neoproterozoic sedimentation along the SW margin of the Congo craton (Kaoko belt, NW Namibia). Gondwana Res. 26, 386–401.
Konopásek, J., Janoušek, V., Oyhantçabal, P., Sláma, J., Ulrich, S., 2018. Did the circum-Rodinia subduction trigger the Neoproterozoic rifting along the Congo–Kalahari Craton margin? Int. J. Earth Sci. 107, 1859–1894.
Konopásek, J., Košler, J., Tajčmanová, L., Ulrich, S., Kitt, S.L., 2008. Neoproterozoic igneous complex emplaced along major tectonic boundary in the Kaoko belt (NW Namibia): ion probe and LA-ICP-MS dating of magmatic and metamorphic zircons. J. Geol. Soc. 165, 153–165.
Korhonen, F.J., Saito, S., Brown, M., Siddoway, C.S., Day, J.M.D., 2010. Multiple generations of granite in the Fosdick mountains, Marie Byrd land, west Antarctica: implications for Polyphase intracrustal differentiation in a continental margin setting. J. Petrol. 51, 627–670.
Kostadinoff, J., 1995. Delimitación de estructuras, litología y espesor de corteza terrestre en áreas continentales y marinas del Sistema de Sierras de Tandilia (Provincia de Buenos Aires). PhD Thesis. Universidad Nacional de La Plata (unpublished), La Plata.
Lara, P., Oyhantçabal, P., Dadd, K., 2016. Post-collisional, late Neoproterozoic, high-Ba-Sr granitic magmatism from the Dom Feliciano belt and its cratonic foreland, Uruguay. In: 8° Congreso Uruguayo de Geología. Actas, Montevideo.
Lara, P., Oyhantçabal, P., Dadd, K., 2017. Post-collisional, Late Neoproterozoic, high-Ba-Sr granitic magmatism from the Dom Feliciano Belt and its cratonic foreland, Uruguay: petrography, geochemistry, geochronology, and tectonic implications. Lithos 277, 178–198.
Leat, P.T., Jackson, S.E., Thorpe, R.S., Stillman, C.J., 1986. Geochemistry of bimodal basalt-subalkaline/peralkaline rhyolite provinces within the Southern British Caledonides. J. Geol. Soc. 143, 259–273.
Lenz, C., Fernandes, L.A.D., McNaughton, N.J., Porcher, C.C., Masquelin, H., 2011. U–Pb SHRIMP ages for the cerro Bori orthogneisses, Dom Feliciano belt in Uruguay: evidences of a ~800 Ma magmatic and ~650 Ma metamorphic event. Precambrian Res. 185, 149–163.
Lenz, C., Porcher, C.C., Fernandes, L.A.D., Masquelin, H., Koester, E., Conceição, R.V., 2013. Geochemistry of the Neoproterozoic (800–767 Ma) cerro Bori orthogneisses, Dom Feliciano belt in Uruguay: tectonic evolution of an ancient continental arc. Mineral. Petrol. 107, 785–806.
Liew, T.C., Hofmann, A.W., 1988. Precambrian crustal components, plutonic associations, plate environment of the Hercynian Fold Belt of central Europe: indications from a Nd and Sr isotopic study. Contrib. Mineral. Petrol. 98, 129–138.
Ludwig, K.R., 2008. User's Manual for Isoplot 3.7. A Geochronological Toolkit for Microsoft Excel, vol. 4 Berkeley Geochronology Center Special Publication, Berkeley.
Martil, M.M.D., Bitencourt, M.F., Nardi, L.V.S., Koester, E., Pimentel, M.M., 2016. Pre-collisional, Neoproterozoic (ca. 790 Ma) continental arc magmatism in southern Mantiqueira Province, Brazil: geochemical and isotopic constraints from the Várzea do Capivarita Complex. Lithos 274, 39–52.
Masquelin, H., Fernandes, L.A.D., Lenz, C., Porcher, C.C., McNaughton, N.J., 2012. The Cerro Olivo Complex: a pre-collisional Neoproterozoic magmatic arc in eastern Uruguay. Int. Geol. Rev. 54, 1161–1183.
McDonough, W.F., Sun, S.-s., 1995. The composition of the Earth. Chem. Geol. 120, 223–253.
Oliveira, D.S., Sommer, C.A., Philipp, R.P., Lima, E.F., Basei, M.A.S., 2015. Post-collisional subvolcanic rhyolites associated to the Neoproterozoic batholith Pelotas, southern Brazil. J. South Am. Earth Sci. 63, 84–100.
Oriolo, S., Becker, T., 2018. The Kalahari craton, southern Africa: from Archean crustal evolution to Gondwana amalgamation. In: Siegesmund, S., Basei, M.A.S., Oyhantçabal, P., Oriolo, S. (Eds.), Geology of Southwest Gondwana. Regional Geology Reviews, Cham, pp. 133–159.
Oriolo, S., Hueck, M., Oyhantçabal, P., Goscombe, B., Wemmer, K., Siegesmund, S., 2018. Shear zones in brasiliano-pan-African belts and their role in the amalgamation and break-up of southwest Gondwana. In: Siegesmund, S., Basei, M.A.S., Oyhantçabal, P., Oriolo, S. (Eds.), Geology of Southwest Gondwana. Regional Geology Reviews, Cham, pp. 593–613.
Oriolo, S., Oyhantçabal, P., Wemmer, K., Basei, M.A.S., Benowitz, J., Pfänder, J., Hannich, F., Siegesmund, S., 2016. Timing of deformation in the Sarandí del Yí Shear Zone, Uruguay: implications for the amalgamation of western Gondwana during the Neoproterozoic Brasiliano-Pan-African Orogeny. Tectonics 35, 754–771.
Oyhantçabal, P., Siegesmund, S., Wemmer, K., 2010b. The Rio de la Plata Craton: a review of units, boundaries, ages and isotopic signature. Int. J. Earth Sci. 100, 201–220.
Oyhantçabal, P., Cingolani, C.A., Wemmer, K., Siegesmund, S., 2018b. The Río de la Plata craton of Argentina and Uruguay. In: Siegesmund, S., Basei, M.A.S., Oyhantçabal, P., Oriolo, S. (Eds.), Geology of Southwest Gondwana. Regional Geology Reviews, Cham, pp. 89–105.
Oyhantçabal, P., Siegesmund, S., Wemmer, K., Layer, P., 2010a. The Sierra Ballena shear zone in the southernmost Dom Feliciano belt (Uruguay): evolution, kinematics, and deformation conditions. Int. J. Earth Sci. 99, 1227–1246.
Oyhantçabal, P., Oriolo, S., Philipp, R.P., Wemmer, K., Siegesmund, S., 2018a. The Nico Pérez terrane of Uruguay and Southeastern Brazil. In: Siegesmund, S., Basei, M.A.S., Oyhantçabal, P., Oriolo, S. (Eds.), Geology of Southwest Gondwana. Regional Geology Reviews, Cham, pp. 161–188.
Oyhantçabal, P., Siegesmund, S., Wemmer, K., Presnyakov, S., Layer, P., 2009. Geochronological constraints on the evolution of the southern Dom Feliciano belt (Uruguay). J. Geol. Soc. 166, 1075–1084.
Oyhantçabal, P., Siegesmund, S., Wemmer, K., Robert, F., Lyer, P., 2007. Post-collisional transition from calc-alkaline to alkaline magmatism during transcurrent deformation in the southernmost Dom Feliciano Belt (Braziliano–Pan-African, Uruguay). Lithos 98, 141–159.
Pángaro, F., Ramos, V.A., 2012. Paleozoic crustal blocks of onshore and offshore central Argentina: new pieces of the southwestern Gondwana collage and their role in the accretion of Patagonia and the evolution of Mesozoic south Atlantic sedimentary basins. Mar. Pet. Geol. 37, 162–183.
Pángaro, F., Ramos, V.A., Pazos, P.J., 2016. The Hesperides basin: a continental-scale upper Palaeozoic to Triassic basin in southern Gondwana. Basin Res. 28, 685–711.
Passarelli, C.R., Basei, M.A.S., Siga Jr., O., Harara, O.M., 2018. The Luis Alves and Curitiba terranes: continental fragments in the Adamastor Ocean. In: Siegesmund, S., Basei, M.A.S., Oyhantçabal, P., Oriolo, S. (Eds.), Geology of Southwest Gondwana.

Regional Geology Reviews, Cham, pp. 189–215.
Passarelli, C.R., Basei, M.A.S., Wemmer, K., Siga Jr., O., Oyhantçabal, P., 2011a. Major shear zones of southern Brazil and Uruguay: escape tectonics in the eastern border of Rio de La Plata and Paranapanema cratons during the Western Gondwana amalgamation. Int. J. Earth Sci. 100, 391–414.
Passarelli, C.R., McReath, I., Basei, M.A.S., Siga Jr., O., Campos Neto, M.C., 2011b. Heterogeneity in syntectonic granitoids emplaced in a major shear zone, southern Brazil. J. South Am. Earth Sci. 32, 369–378.
Pearce, J.A., Cann, J.R., 1973. Tectonic setting of basic volcanic rocks determined using trace element analyses. Earth Planet. Sci. Lett. 19, 290–300.
Pearce, J.A., Harris, N.B.W., Tindle, A.G., 1984. Trace element discrimination diagrams for the tectonic interpretation of granitic rocks. J. Petrol. 25, 956–983.
Peccerillo, A., Taylor, S.R., 1976. Geochemistry of Eocene calc-alkaline volcanic rocks from the Kastamonu area, Northern Turkey. Contrib. Mineral. Petrol. 58, 63–81.
Pedrosa-Soares, A.C., Alkmim, F.F., Tack, L., Noce, C.M., Babinski, M., Silva, L.C., Martins-Neto, M.A., 2008. Similarities and differences between the Brazilian and African counterparts of the Neoproterozoic Araçuaí-west Congo orogen. In: In: Pankhurst, R.J., Trouw, R.A.J., Brito Neves, B.B., de Wit, M.J. (Eds.), West Gondwana: Pre-cenozoic Correlations across the South Atlantic Region, vol. 294. Geological Society Special Publications, London, pp. 153–172.
Peucat, J.J., Vidal, P., Bernard-Griffiths, J., Condie, K.C., 1989. Sr, Nd, and Pb isotopic systematics in the Archean low- to high-grade transition zone of southern India: syn-accretion vs. Post-accretion Granulites. J. Geol. 97, 537–549.
Prezzi, C.B., Vizán, H., Vázquez, S., Renda, E., Oriolo, S., Japas, M.S., 2018. Evolution of the Paleozoic Claromecó Basin (Argentina) and geodynamic implications for the southwestern margin of Gondwana: insights from isostatic, gravimetric and magnetometric models. Tectonophysics 742–743, 120–136.
Philipp, R.P., Lusa, M., Nardi, L.V.S., 2008. Geochemistry and petrology of dioritic, tonalitic and trondhjemitic gneisses from Encantadas Complex, Santana da Boa Vista, southernmost Brazil, a Paleoproterozoic continental-arc magmatism. An Acad. Bras Ciências 80, 1–14.
Philipp, R.P., Machado, R., Chemale Jr., F., 2003. Reavaliação e novos dados geocronológicos sobre o Batólito Pelotas: implicações petrogenéticas e idade das zonas de cisalhamento. Boletim do Instituto de Geociências da USP 3, 71–84.
Philipp, R.P., Massone, H.J., Campos, R.S., 2013. Peraluminous leucogranites of Cordilheira suite, record of Neoproterozoic collision and generation of Pelotas batholith, Dom Feliciano belt, southern Brazil. J. South Am. Earth Sci. 43, 8–24.
Philipp, R.P., Pimentel, M.M., Chemale Jr., F., 2016a. Tectonic evolution of the Dom Feliciano belt in southern Brazil: geological relationships and U-Pb geochronology. Braz. J. Geol. 46, 83–104.
Philipp, R.P., Machado, R., Nardi, L.V.S., Lafon, J.M., 2002. O magmatismo granítico Neoproterozóico do Batólito Pelotas no sul do Brasil: novos dados e revisão de geocronologia regional. Rev. Bras. Geociencias 32, 277–290.
Philipp, R.P., Bom, F.M., Pimentel, M.M., Junges, S.L., Zvirtes, G., 2016b. SHRIMP U-Pb age and high temperature conditions of the collisional metamorphism in the Varzea do Capivarita Complex: implications for the origin of Pelotas Batholith, Dom Feliciano Belt, southern Brazil. J. South Am. Earth Sci. 66, 196–207.
Porada, H., Berhorst, V., 2000. Towards a new understanding of the Neoproterozoic–early Paleozoic Lufilian and northern Zambezi belts in Zambia and the Democratic Republic of Congo. J. Afr. Earth Sci. 30, 727–771.
Preciozzi, F., Masquelin, H., Basei, M.A.S., 1999. The Namaqua/Grenville terrane of eastern Uruguay. In: 2° South American Symposium on Isotope Geology. Córdoba, Actas, pp. 338–340.
Ramos, V.A., Chemale Jr., F., Naipauer, M., Pazos, P.J., 2014. A provenance study of the Paleozoic Ventania system (Argentina): Transient complex sources from western and eastern Gondwana. Gondwana Res. 26, 719–740.
Rapela, C.W., Pankhurst, R.J., Fanning, C.M., Grecco, L.E., 2003. Basement evolution of the Sierra de la Ventana Fold Belt: new evidence for Cambrian continental rifting along the southern margin of Gondwana. J. Geol. Soc. 160, 613–628.
Rapela, C.W., Fanning, C.M., Casquet, C., Pankhurst, R.J., Spalletti, L., Poiré, D., Baldo, E.G., 2011. The Rio de la Plata craton and the adjoining Pan-African/brasiliano terranes: their origins and incorporation into south-west Gondwana. Gondwana Res. 20, 673–690.
Rapela, C.W., Pankhurst, R.J., Casquet, C., Fanning, C.M., Baldo, E.G., González-Casado, J.M., Galindo, C., Dahlquist, J., 2007. The Río de la Plata craton and the assembly of SW Gondwana. Earth Sci. Rev. 83, 49–82.
Sato, K., Tassinari, C.C.G., Kawashita, K., Petronilho, L., 1995. O método geocronológico Sm-Nd no IG/USP e suas aplicações. An Acad. Bras Ciências 67, 313–336.
Schiller, W., 1930. Investigaciones geológicas en las montañas del sudoeste de la provincia de Buenos Aires. Anales del Museo de La Plata, Tomo 4, 2–101.
Shand, S.J., 1927. On the relations between silica, alumina, and the bases in eruptive rocks, considered as a means of classification. Geol. Mag. 64, 446–449.
Silva, L.C., Hartmann, L.A., McNaughton, N.J., Fletcher, I.R., 1999. SHRIMP U/Pb zircon dating of Neoproterozoic granitic magmatism and collision in the Pelotas batholith, southernmost Brazil. Int. Geol. Rev. 41, 531–551.
Sommer, C.A., Fernandes de Lima, E., Nardi, L.V.S., Figueiredo, A.M.G., Pierosan, R., 2005. Potassic and low- and high-Ti mildly alkaline volcanism in the Neoproterozoic Ramada Plateau, southernmost Brazil. J. South Am. Earth Sci. 18, 237–254.
Sommer, C.A., Leitzke, F.P., Fernandes de Lima, E., Santos Barreto, C.J., Lafon, J.M., Matté, V., Philipp, R.P., Conceição, R.V., Basei, M.A.S., 2017. Zircon U–Pb geochronology, Sm–Nd and Pb–Pb isotope systematics of Ediacaran post-collisional high-silica Acampamento Velho volcanism at the Tupanci area, NW of the Sul-Rio-Grandense Shield, Brazil. Braz. J. Geol. 47, 545–560.
Souza, S.L., Basei, M.A.S., Sato, K., Silva, W.B., 2017. LA-MC-ICP-MS instrumentation and acquisition of U-Pb ages on zircon, monazite and titanite at CPGeo-USP. In: 2° Workshop of Inorganic Mass Spectrometry, São Paulo, available at: http://wims.igc.usp.br/wp-content/uploads/2017/07/Solange-Lucena-2-1.pdf.
Stacey, J.S., Kramers, J.D., 1975. Approximation of terrestrial lead isotope evolution by a two-stage model. Earth Planet. Sci. Lett. 26, 207–221.
Suero, T., 1972. Compilación geológica de las Sierras Australes de la Provincia de Buenos Aires. Anales LEMIT (La Plata), Serie 2, 135–147.
Sun, S.-s., McDonough, W.F., 1989. Chemical and isotopic systematics of oceanic basalts: implications for mantle composition and processes. In: In: Saunders, A.D., Norry, M.J. (Eds.), Magmatism in the Ocean Basins, vol. 42. Geological Society Special Publications, London, pp. 313–345.
Thomas, R.J., Macey, P.H., Spencer, C., Dhansay, T., Diener, J.F.A., Lambert, C.W., Frei, D., Nguno, A., 2016. The Sperrgebiet domain, Aurus mountains, SW Namibia: a ~2020–850 Ma window within the pan-African Gariep orogen. Precambrian Res. 286, 35–58.
Tohver, E., Cawood, P.A., Rossello, E.A., Jourdan, F., 2012. Closure of the Clymene Ocean and Formation of west Gondwana in the Cambrian: evidence from the sierras Australes of the southernmost Rio de la Plata craton, Argentina. Gondwana Res. 21, 394–405.
Tomezzoli, R.N., 2001. Further palaeomagnetic results from the Sierras Australes fold and thrust belt, Argentina. Geophys. J. Int. 147, 356–366.
Tomezzoli, R.N., Vilas, J.F., 1999. Paleomagnetic constraints on age of deformation of the Sierras Australes thrust and fold belt, Argentina. Geophys. J. Int. 138, 857–870.
Umpierre, M., Halpern, M., 1971. Edades Rb-Sr del Sur de la República Oriental del Uruguay. Rev. Asoc. Geol. Argent. 26, 133–155.
Uriz, N.J., Cingolani, C.A., Chemale Jr., F., Macambira, M.B., Armstrong, R., 2011. Isotopic studies on detrital zircons of Silurian–Devonian siliciclastic sequences from Argentinean North Patagonia and Sierra de la Ventana regions: comparative provenance. Int. J. Earth Sci. 100, 571–589.
Varela, R., Cingolani, C.A., 1976. Nuevas edades radimétricas del basamento aflorante en el Perfil del Cerro Pan de Azúcar-Cerro del Corral y consideraciones sobre la evolución geocronológica de las rocas ígneas de las Sierras Australes, Provincia de Buenos Aires. In: 6° Congreso Geológico Argentino, vol. 1. Actas, Buenos Aires, pp. 543–556.
Varela, R., Cingolani, C., Dalla Salda, L.H., 1990. Edad del granito Cerro Colorado y su implicancia geotectónica. Sierras Australes de Buenos Aires. In: 11° Congreso Geológico Argentino, vol. 2. Actas, Buenos Aires, pp. 279–282.
Varela, R., Dalla Salda, L.H., Cingolani, C.A., 1985. Estructura y composición geológica de las sierras Colorada, Chasicó y Cortapié, Sierras Australes de Buenos Aires. Rev. Asoc. Geol. Argent. 40, 254–261.
von Gosen, W., Buggisch, W., Dimieri, L.V., 1990. Structural and metamorphic evolution of the sierras Australes (Buenos Aires Province/Argentina). Geol. Rundsch. 79, 797–821.
von Gosen, W., Buggisch, W., Krumm, S., 1991. Metamorphism and deformation mechanisms in the sierras Australes fold and thrust belt (Buenos Aires Province, Argentina). Tectonophysics 185, 335–356.
Whalen, J.B., Currie, K.L., Chappell, B.W., 1987. A-type granites: geochemical characteristics, discrimination and petrogénesis. Contrib. Mineral. Petrol. 95, 407–419.
Will, T.M., Gaucher, C., Ling, X.-X., Li, X.-H., Li, Q.-L., Frimmel, H.E., 2019. Neoproterozoic magmatic and metamorphic events in the Cuchilla Dionisio terrane, Uruguay, and possible correlations across the south Atlantic. Precambrian Res. 320, 303–322.
Winchester, J.A., Floyd, P.A., 1977. Geochemical discrimination of different magma series and their differentiation products using immobile elements. Chem. Geol. 20, 325–343.
Wood, D.A., 1980. The application of a Th-Hf-Ta diagram to problems of tectonomagmatic classification and to establishing the nature of crustal contamination of basaltic lavas of the British Tertiary Volcanic Province. Earth Planet. Sci. Lett. 50, 11–30.
Zavala, C., Azúa, G., Freije, R.H., Ponce, J.J., 2000. Sistemas deltaicos dominados por evenidas fluviales en el Grupo Curamalal (Paleozoico inferior), Cuenca paleozoica de Ventania, provincia de Buenos Aires, Argentina. Rev. Asoc. Geol. Argent. 55, 165–178.